



DELFT UNIVERSITY OF TECHNOLOGY

BACHELOR THESIS

**Persistent structures
in a shallow cumulus cloud field**

Author:
C.E. DE WINTER

Supervisors:
Dr. S.R. DE ROODE
J.J. VAN DER DUSSEN

May 16, 2012

Abstract

The main research goal of this thesis was to find persistence in a shallow cumulus cloud field. To be able to qualitatively and quantitatively evaluate this persistence different approaches are used.

Basis for this research are the measurements done during the atlantic stratocumulus to cumulus transition experiment (also known as ASTEX). Results from these measurements are modelled by J.J. van der Dussen using DALES. Final dataset used is based on hours 29 till 32 of the ASTEX-case, containing a domain of 4.5 by 4.5km and a height of 2.2km. This domain was subdivided in a grid of 128x128x350 points, while time was subdivided in steps of each 30 seconds.

Final result is based on four main points:

- Persistence is found that shows a time scale of more than one hour by visual inspection of time-averaged surface plots. This time scale is significant compared to estimated the life time of the clouds of 30 minutes. Another approach calculating the cloud presence shows also that clouds with a minimum liquid water path of 0.1 kg.m^{-2} are present during a non-consecutive time of one hour and ten minutes. Average cloud presence in this field was 7 minutes.
- A strong anti correlation between the specific water content and (virtual) potential temperature is found in time-averaged surface plots. In this report only the results at 1km are shown, but this anti correlation is shown at each height.
- The vertical velocity shows downdrafts of 0.2 m.s^{-1} in the time average over four hours of measurements. These strong downdrafts are found where liquid water content and specific total water content is low.
- The largest integral time scale is 55 minutes, found for the total specific water content. The reliability of this integral time scale is however doubtful, because of the periodic boundary conditions that could influence the integral time scale. This could be improved if a domain is used that is larger than eight times the integral length scale. Integral length scale can be calculated from the integral time scale by multiplying it with the horizontal velocity. This results in a recommended domain of 100km in each direction.

Contents

1	Introduction	5
1.1	Background	5
1.2	Persistence based on cloud formation	8
1.3	Research question and Hypothesis	9
1.4	Structure of the report	9
2	Theory	11
2.1	Atmospheric Physics	11
2.1.1	Moisture variables	11
2.1.2	Virtual temperature	12
2.1.3	Potential temperature	13
2.1.4	Equivalent potential temperature	14
2.1.5	The adiabatic lapse rate	15
2.2	Cumulus Clouds	16
2.2.1	Stable or unstable atmosphere	16
2.2.2	Development of cumulus clouds	17
2.3	Dutch Atmospheric LES-model	20
2.4	Mathematical Tools	21
2.4.1	Autocorrelation	21
2.4.2	Integral timescale	22
3	Setup	25
3.1	LES domain	25
3.2	Considerations	25
3.2.1	Cloud base and top	25
3.2.2	Life time of a cloud	25
3.2.3	Lagrangian translation of the 3D field	25
3.3	Rough approach	26
3.3.1	Cloud presence	26
3.3.2	Cloud fraction	29
3.4	Time averaging	29
3.4.1	Expectations	29
3.4.2	Evaluation	32
3.5	Summary and look ahead	33
4	Autocorrelation	35
4.1	Introduction	35
4.2	Expectations	36
4.3	Linear trend of the variables	36
4.4	Autocorrelation and integral timescale	37
4.4.1	Integral time scale surface plots	40
4.5	Summarized results	43
5	Conclusion and discussion	45
5.1	Recommendations	46

Abbreviations	48
Symbols	48
References	50
A Time-averaged profiles	52
A.1 Specific total water content	52
A.2 Specific rain content	53
A.3 Potential temperature	54
A.4 Virtual potential temperature	55
A.5 Vertical velocity	56
A.6 Total water path	57

Chapter 1

Introduction

1.1 Background

Clouds interact in many different processes, for instance radiation, microphysics, turbulent transport through the atmosphere and evaporation and condensation of water. Radiation by clouds plays an important role in the heating of the earth and atmosphere by the sun. The visibility and radiative properties of clouds are caused by light scattering on droplets of liquid water in the air. It is easy to understand that a blanketed of clouds isolates the earth from external influences like sunshine, while non-area covering clouds like cumulus are often related to a more dynamic atmosphere. More specific, a solid layer of stratocumulus clouds reflects about 90% of the shortwave radiation, while cumulus clouds reflect about 10%.

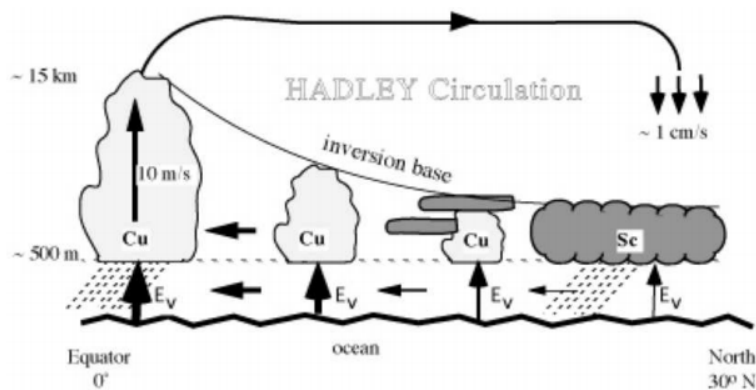


Figure 1.1.1: Schematic drawing of the hadley circulation cell. E_v stands for the water evaporation from the ocean's surface, Sc is stratocumulus, Cu cumulus, or in leftmost figure Cumulonimbus. Note the difference in evaporation at the equator and at 30 degrees North indicated with the thickness of the arrows E_v .

Between the subtropics and the tropics, a dense layer of clouds moving towards the equator slowly evolves into a thin layer penetrated by cumulus clouds. At the point the moving air reaches the tropics often large precipitative clouds are found. This phenomenon is part of the Hadley circulation, schematically drawn in figure 1.1.1. The Hadley circulation is a large scale circulation of air. Due to this circulation moist and cloudy air in the lower regions of the atmosphere moves towards the equator. At the equator a strong updraft of air is shown caused by heating and evaporation of water. Air in the uppermost regions of the atmosphere again moves towards the subtropics while cooling down.

To gain more insight on the evolution of the stratocumulus evolving into the cumulus clouds, the Atlantic Stratocumulus Transition EXperiment, abbreviated ASTEX, was performed. In this experiment during June 1992, two consecutive days of measurements have taken place near the Canary Islands.

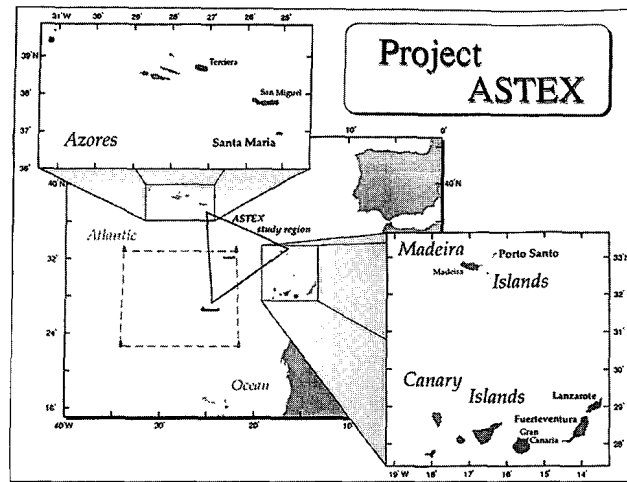


Figure 1.1.2: Schematic picture of the region where the large field experiment ASTEX took place. The two enlarged square regions give a view on the Madeira's and Azores, islands from where ground based observations and air craft operations have been performed. [1]

During two consecutive days of measurements, a cloud mass is followed while transitioning from stratocumulus (a low, grey blanket of contingent clouds), slowly evolving via a thin, broken stratocumulus layer penetrated from below by cumulus clouds to cumulonimbus. Cumulonimbus clouds are big precipitative clouds, while cumulus clouds are often smaller and do not contain rain. Measurements have been done with satellites, marine instruments and planes flying under, through, and above clouds.

One of the ASTEX flights (Flight A210) consisted of 8 consecutive horizontal runs through roughly the same air mass. The observations showed that a cumulus cloud was present during one hour of measuring. This is also shown in figure 1.1.3. [2]

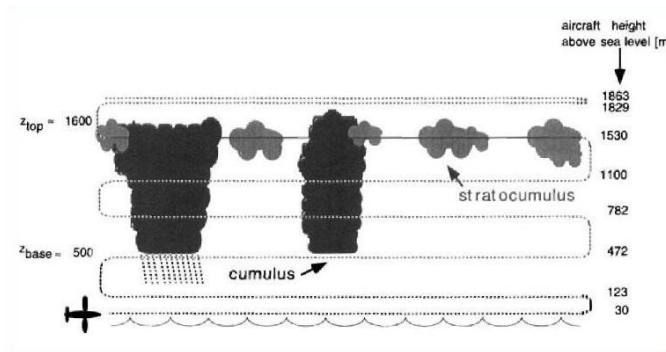


Figure 1.1.3: Schematic picture of flight A210, run the 14th of June between 11.11 and 13.02 (UTC). The airplane starts at a low height and during the flight through the same mass of air it increases height. The cumulus cloud appeared to be persistent during the one hour measurement. Figure copied after [2].

The measurements done in the ASTEX project form a basis for computational simulations of the processes taking place in the atmosphere. An example of such a model is the Large Eddy Simulation model, which can resolve larger turbulence scales (ranging from meters up to a few km) [3]. In these larger ranges most of the turbulent transport occurs. An LES model can thus be used to simulate the measured variables into a 3D cloud field containing the most important variables.

In this project data generated with an LES model is analysed. The area of interest is limited to the transition of the thin layer of broken stratocumulus towards the persistent cumulus as observed in flight A210. This means that we are looking at hours 22.20 - 1.20 on June 13-14 of the ASTEX case. Of this time no flight data is known, as can be seen in figure 1.1.4.

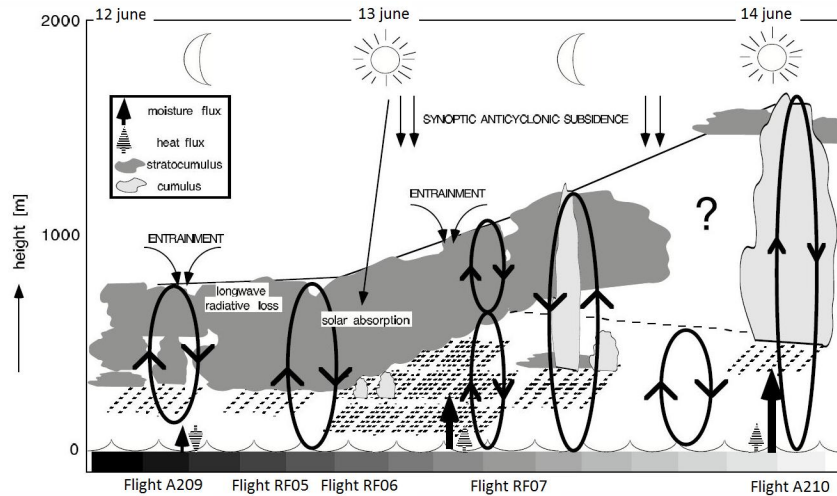


Figure 1.1.4: Figure on the transition from stratocumulus via shallow cumulus penetrating the thinning stratocumulus layer to cumulonimbus as observed during ASTEX. The area of interest for this research project is the transition zone between shallow cumulus and persistent cumulonimbus located at the question mark, where no specific flight data is found. Figure made after [4].

1.2 Persistence based on cloud formation

The formation of a cloud starts with the rising of warm and moist air, often called a thermal. Under certain conditions a thermal reaches a point where condensation takes place, the exact conditions will be explained further in section 2.2, and lead to the expectation that a cloud has a bigger chance to evolve at a location a cloud has existed before.

This is shortly explained based on the following process; if a shallow cloud is formed, lateral mixing takes place at the edges of that cloud. This lateral mixing causes evaporation of the cloud. Gradually, the cloud disappears, leaving an area that contains more moist and a lower air temperature compared to the environmental air. These conditions a previous cloud has left in the atmosphere could make the difference between condensation of the moist of a 'new' thermal or not condensing it. In other words, the environment as left behind by previous clouds could make the difference between reaching circumstances where a new cloud is formed or not.

Recently, Dawe and Austin investigated how initial atmospheric conditions influence formations of shallow cumulus [5]. They used an LES simulation of a shallow cumulus cloud field based upon the Barbados Oceanographic and Meteorological Experiment (BOMEX). They concluded that *'cloud thermodynamic properties are primarily influenced by entrainment and detrainment processes, cloud area and height are primarily influenced by cloud base area, and thus nature and nurture both play roles in the dynamics of BOMEX shallow cumulus clouds.'* In this conclusion 'nature' are the properties at cloud base that possibly determine the upper-level properties, while 'nurture' stands for the properties determined by the environmental conditions thermals might encounter. The entrainment and detrainment is part of the environment a thermal encounters, and

could be induced by clouds that have existed before. Therefore, it can be part of the 'nurture' of a cloud. Nothing is said about this by Dawe and Austin however.

1.3 Research question and Hypothesis

If it is indeed more likely to find a cloud where a cloud has existed before, this should be visible in the LES data. The basic research aim of this project is to find the relation between previous clouds and the presence of later formed clouds. While following the same air mass, autocorrelation of thermodynamic variables in time is calculated. An estimated lifetime of cumulus clouds is used as a reference value to evaluate whether these thermodynamic properties are persistent over a significant time scale. We expect that this time scale will be significantly larger than the typical 30min lifetime of shallow cumulus in these fields. Finally, with these results we hope to get to know something more about the persistent structures in the transition zone from stratocumulus to cumulus. Therefore the results will be compared to the basic observations made during the ASTEX flights RF07 and A210, to check the reliability of the LES model used in this project.

1.4 Structure of the report

In chapter 2, most important variables and formulas are deduced or explained. This chapter gives more theoretical background information on heat and moisture, specific moist content and temperature scales. Different atmospheric variables will be derived, and it will be explained how they influence cloud formation. Next to that, a short explanation on the numerical Large Eddy Simulations is given. Chapter 2 also contains the mathematical tools and numerical approaches used in this report; about how autocorrelation and integral time scale are calculated.

In chapter 3 the derivation of the existence of persistent structures is made. Starting with an estimation of the cloud fraction and cloud cover, and by averaging the fields over time. These results form a basis for calculating the autocorrelation of different variables in time, which is done in chapter 4.

Chapter 2

Theory

2.1 Atmospheric Physics

In the atmosphere of the earth, many different physical processes take place. These processes are modelled by physicist in order to describe and predict among others turbulent transport of heat, moisture and air pollution. In this section, most important variables and processes of (shallow) cumulus clouds are explained. The theory in this section is based on the explanations given by Wallace and Hobbs, de Roode, and Axelsen [6, 7, 8].

2.1.1 Moisture variables

Specific humidity and mixing ratio

The atmosphere mainly contains Nitrogen and Oxygen, 78.08 respectively 20.95 Vol % of the air. Water vapor is 0 to 5 Vol % of the atmosphere [9]. Although this small volume percentage, the moisture content plays an important role in cloud physics; the presence of moist causes clouds to evolve.

In meteorology, dimensionless measures are used to describe the moisture content. Specific humidity q_k for instance, is the ratio of moist mass m_k to the total mass of a volume of air m , calculated via:

$$q_k = \frac{m_k}{m} \quad (2.1)$$

In equation(2.1) the subscript k can be replaced by v , l or i standing for water in the vapor, liquid or ice phase respectively. The term m_k is the total mass of water in the state specified by its subscript k . The total specific humidity or specific total water content is defined by adding the three terms:

$$q_t = q_v + q_l + q_i \quad (2.2)$$

Liquid water path

The liquid water path W is the total amount of liquid water between two vertical levels in the atmosphere. It is an important quantity in the radiative transfer in the atmosphere, and above that a way to express the spatial coverage of (liquid water) clouds. A higher liquid water path means more reflection of solar radiation. This reflection property is used in observing the atmosphere with satellites. The liquid water path W is defined as:

$$W = \int_0^{\text{inf}} \rho_{air} q_l dz \quad (2.3)$$

The upper integration limit is in our case the top of the LES domain, ρ_{air} the density of air, which is assumed have a constant value of 1.2 kgm^{-3} with height. A variation on

the liquid water path is the total water path. For the total water path q_t is integrated over height:

$$W = \int_0^{\text{inf}} \rho_{air} q_t dz \quad (2.4)$$

Relative Humidity

The relative humidity RH of air is defined as the ratio of the water vapor pressure e and the saturation vapor pressure e_s :

$$RH = \frac{e}{e_s} \quad (2.5)$$

2.1.2 Virtual temperature

The universal gas law is applied in order to evaluate the pressure, density and temperature of a volume of air. The gas law can be rewritten from $pV = nR^*T$, with R^* the universal gas constant, V the volume of the evaluated n moles of gas at pressure p , into

$$p_d = \rho_d R_d T \quad (2.6)$$

In equation(2.6) p_d is the pressure in case of dry air, ρ_d is the density of dry air and R_d is the gas constant of dry air, equal to $287 \text{ Jkg}^{-1}\text{K}^{-1}$ and defined as:

$$R_d = \frac{nR^*}{\rho_d V} \quad (2.7)$$

For an air-moisture mixture, a comparable relation can be deduced. The partial vapor pressure e is similarly calculated via:

$$e = \rho_v R_v T \quad (2.8)$$

Moist air has a smaller apparent specific weight then dry air. This means that a volume of moist air is lighter than a volume of dry air at the same actual temperature and pressure. Vapor content varies considerably, therefore instead of using a variable gas constant, it is proven to be more workable to use the gas constant for dry air together with a fictive temperature; the virtual temperature.

The virtual temperature T_v is the temperature that air of a given pressure and density would have if this air was completely free of water. In this way, virtual temperature is always greater than the actual temperature, because moist air is less dense than dry air at the same temperature and pressure.

Virtual temperature is deduced starting at the influence of liquid water on the pressure. Total pressure p is:

$$p = p_d + e = \rho R_m T = \rho_d R_d T + \rho_v R_v T \quad (2.9)$$

Using $q_v = \frac{\rho_v}{\rho}$ and $\rho_d = 1 - q_v - q_l$ the gas constant R_m for the mixture can be written as:

$$R_m = (1 - q_v - q_l)R_d + q_v R_v \quad (2.10)$$

Writing $p = \rho R_m T = \rho R_d T_v$ gives the virtual temperature T_v

$$T_v = [1 - (1 - 1/\epsilon)q_v - q_l]T \quad (2.11)$$

With $\epsilon = \frac{R_d}{R_v} \approx 0.622$.

The difference between virtual and actual temperature is only a few degrees.

2.1.3 Potential temperature

Starting from a parcel's given pressure and temperature, the parcel is (imaginary) expanded or compressed adiabatically to a standard pressure p_0 , usually $p_0 = 1000\text{hPa}$. The temperature the parcel would have in this state is named the potential temperature θ . The derivation of this potential temperature is explained in this section, starting with an adiabatic process. In an adiabatic process, the first law of thermodynamics can be described as:

$$c_p dT - \alpha dp = dq = 0 \quad (2.12)$$

In which α is defined via the universal gas law as $\frac{1}{\rho}$. The gas law is then written as $p\alpha = RT$. And thus, equation (2.12) can be integrated from p_0 (where $T' = \theta$) to p (where $T' = T$) resulting in:

$$\frac{c_p}{R_d} \int_{\theta}^T \frac{dT'}{T'} = \int_{p_0}^p \frac{dp}{p} \quad (2.13)$$

Evaluating and rewriting equation (2.13) then gives Poissoins equation:

$$\theta = T \left(\frac{p_0}{p} \right)^{\frac{R_d}{c_p}} \quad (2.14)$$

Atmospheric processes are close to adiabatic for parcels that are displaced vertically by atmospheric flow, therefore θ remains essentially constant. This makes the potential temperature a useful parameter in atmospheric thermodynamics. How potential temperature is an important stability parameter will be shown later in this chapter.

Virtual potential temperature

A similar derivation of the virtual temperature leads to the virtual potential temperature θ_v

$$\theta_v = T_v \left(\frac{p_0}{p} \right)^{\frac{R_d}{c_p}} \quad (2.15)$$

Combining equations (2.11), (2.14) and (2.15) gives:

$$\theta_v = [1 - (1 - 1/\epsilon)q_v - q_l] \theta \quad (2.16)$$

Since $\epsilon = 0.622$, and $q_v = q_t - q_l$ (assuming q_i is negligibly small) this can be simplified to:

$$\theta_v = \theta [1 + 0.61q_t - 1.61q_l] \quad (2.17)$$

Clausius-Clapeyron equation

The Clausius-Clapeyron equation describes how the saturated vapor pressure of a liquid changes with temperature. It can be derived from the Carnot cycle with a liquid and its saturated vapor. For the exact derivation, see Wallace and Hobbs [10]. The Clausius-Clapeyron equation is:

$$\frac{de_s}{dT} = \frac{L_v}{T(\alpha_2 - \alpha_1)} \quad (2.18)$$

In this equation, L_v is the heat released or absorbed by a body during a change of state without change of temperature. In case of evaporation α_1 and α_2 are the specific volumes in liquid phase (1) and in vapor phase (2) at temperature T , respectively. $(\alpha_2 - \alpha_1)$ is thus the change in volume of the considered system changing from state 1 to state 2.

2.1.4 Equivalent potential temperature

The equivalent potential temperature θ_e of an air parcel is used to describe rising moist air parcels. Equivalent potential temperature is conserved for adiabatic displacements inducing phase changes of water. Following the Clausius-Clapeyron equation (2.18), the saturation vapor pressure of a moist air parcel will decrease during the isentropic rising of the parcel (an isentropic process is a process with constant entropy). This means that the maximum amount of vapor a parcel can contain decreases with height. At a certain height, the water vapor pressure in a parcel is equal to its saturation value. While the particle still increases height, liquid water will condense resulting in a release of latent heat. Latent heat however is not released to the atmosphere, but absorbed by the parcel itself. This process makes that the potential temperature of the parcel increases with height.

The equivalent potential temperature θ_e takes this effect into account, and therefore remains constant for isentropic processes involving phase changes. It can be derived in a similar way as the potential temperature, taking into account the energy exchange with the environment in the form of latent heat release. This finally results into:

$$\theta_e \approx \theta \cdot e^{\frac{L_v q_v}{c_p T}} \quad (2.19)$$

In equation (2.19), w_s is the saturation mixing ratio, defined as ratio of the mass of water vapor to the mass of dry air in a given volume of air that is saturated with respect to a plane surface of pure water.

Equation (2.19) can be further approximated using Taylor expansion and the assumption that the argument in the exponent is sufficiently small:

$$\theta_e \approx \theta + \frac{L_v}{c_p} q_v \quad (2.20)$$

The equivalent potential temperature is conserved during both dry and saturated adiabatic processes.

Liquid water potential temperature

Another quantity that is conserved for isentropic processes including phase changes is the liquid water potential temperature,

$$\theta_l \approx \theta - \frac{L_v}{c_p} q_l \quad (2.21)$$

2.1.5 The adiabatic lapse rate

If a material changes in physical state (for instance pressure, volume or temperature) without the exchange of heat with the environment taking place, the change is called adiabatic. The adiabatic lapse rate is the rate temperature changes, while a parcel of air rises or descends in the atmosphere.

Dry adiabatic lapse rate

The dry adiabatic lapse rate is found under three important conditions: a dry air parcel has to move adiabatically through the atmosphere, it should move slow enough so that macroscopic kinetic energy is a negligible fraction of its total energy. And finally, the atmosphere has to be in hydrostatic equilibrium. If (the movement of) a parcel meets all these conditions, the parcel's temperature will follow the dry adiabatic lapse rate. The change in internal energy for a unit mass in the parcel can be written as:

$$d(c_p T + \Phi) = 0 \quad (2.22)$$

In this equation, c_p is the heat capacity at constant pressure, and Φ is the gravitational potential energy per unit mass. This means $\frac{d\Phi}{dz} = g$. Dividing (2.22) through by dz gives:

$$-\left(\frac{dT}{dz}\right)_{dryparcel} = \frac{g}{c_p} \equiv \Gamma_d \quad (2.23)$$

In (2.23), Γ_d is the dry adiabatic lapse rate, the rate of temperature change of a unit mass of dry air that is moving vertically and adiabatically in the atmosphere.

Wet adiabatic lapse rate

It is also possible to derive a wet adiabatic lapse rate Γ_m for a moist air parcel under the same conditions as stated in the derivation of the dry adiabatic lapse rate. In this case, liquid water potential temperature θ_l and the total water content q_t are assumed to be constant as well, leading to:

$$\frac{d\theta}{dz} + \frac{l_v}{c_p} \frac{dq_s}{dz} = 0 \quad (2.24)$$

The wet adiabatic lapse rate can be written as [11]:

$$\Gamma_m = -\frac{dT}{dz} = \Gamma_d \left[\frac{1 + \frac{q_s L_v}{R_d T}}{1 + \frac{L_v^2 q_s}{c_p R_v T^2}} \right] < \Gamma_d \quad (2.25)$$

2.2 Cumulus Clouds

Cumulus clouds are known in different forms, most characteristic for cumulus clouds is their puffy white or light gray appearance. Cumulus clouds have a flat bottom, and sharp outlines. The individual clouds develop most often vertically, starting from a cloud base height of about 1km. Having a width of about 1-2km, shallow cumulus is often non-precipitative, although there are (bigger) cumulus clouds that do contain rain. In this chapter however, precipitation will not be taken into account in the dynamics; the so called fair weather cumulus is described, and evaluated.



Figure 2.2.1: Cumulus clouds developing as observed from an airplane flying above the Atlantic Ocean at a height of 3km. This picture is taken during noon looking westward. The island seen in the picture is Barbados. This picture has been taken during a test flight of the Carriba project 2010-2011 [12].

2.2.1 Stable or unstable atmosphere

The vertical mixing of the atmosphere is an important factor in the development of cumulus clouds. Most important in defining stability of the atmosphere is the buoyancy of the different air layers, which can be expressed via the virtual temperature, and more precisely how virtual temperature changes with height. One assumption that is done in following argumentation is:

$$\frac{d\bar{T}_v}{dz} \approx \frac{d\bar{T}}{dz} \quad (2.1)$$

In this equation the effect of moisture on the vertical gradient of T_v is neglected. There are three main conditions of the atmosphere; the first condition is mainly found at night, when radiative heating of the sun does not take place. In this condition, the heaviest air stays at the surface and virtual temperature increases with height; the atmosphere is 'stable', this state is also known as stable stratification. Comparing the mean temperature lapse rate with the wet adiabatic lapse rate gives that the mean temperature lapse rate is smaller than the wet-adiabatic lapse rate. This means that both dry and wet convection will be damped. In formula, the absolute stable stratification is

known as:

$$-\frac{d\overline{T}_v}{dz} < \Gamma_{\theta_v} < \Gamma_d \quad (2.2)$$

In this equation Γ_d is defined as $\frac{d\theta_v}{dz}=0$, and $\Gamma_{\theta_v} \equiv \left(\frac{d\theta_v}{dz}\right)_{moist,adiabatic} > 0$. The second condition is unstable stratification; in this condition the top of the atmosphere has a negative buoyancy gradient; $\frac{dT}{dz} < 0$, at the top virtual temperature decreases with height. This condition is caused by heating of the atmosphere near the earth, whereby the air close to earth becomes less dense than the air at higher layers of the atmosphere. In this condition of the atmosphere, the mean temperature lapse rate is even smaller than the dry-adiabatic lapse rate. Any air will rise; the atmosphere is unstable. The unstable stratification can be written in terms of the temperature lapse rate via:

$$-\frac{d\overline{T}}{dz} > \Gamma_d \quad (2.3)$$

Another possibility is conditional instability of the atmosphere, in this case:

$$\Gamma_m < -\frac{d\overline{T}}{dz} < \Gamma_d \quad (2.4)$$

Rising thermals in a conditionally unstable layer will only rise further if they contain enough moisture to reach saturation vapor pressure within the conditional unstable layer. Reaching saturation vapor pressure causes condensation of water. The heat released by this condensation increases the temperature of the thermal; the thermal gains a higher virtual temperature than the environment. A higher virtual temperature than the environment results in an upward directed buoyancy, the thermal therefore can move through the conditional unstable layer. A thermal that does not contain enough moisture will be stopped in this layer due to the temperature gradient of the atmosphere.

The third condition is a well mixed atmosphere, resulting in a virtual temperature lapse rate and density that both do not change with height.

2.2.2 Development of cumulus clouds

The development of a cumulus cloud starts with the decrease of density of the air near the earth surface. This density change can be caused by solar warming of the ground surface, or evaporation of moist from the earth surface. A moist parcel is lighter than a dry parcel; if moist has evaporated from earth surface the closest layer of air is moist, and therefore lighter.

Because of the difference in density with respect to a higher layer, the lighter air starts to rise. This rising air is called a thermal. If it is assumed that the thermal rises without mixing with the environment, it rises adiabatically. During this rising, the temperature of the thermal will follow the dry adiabatic lapse rate Γ_d , meaning that its temperature will increase linearly with height.

The virtual temperature can be used to calculate the net buoyant force on the particle via the Boussinesq approximation. Following Rogers and Yau [13] the Boussinesq approximation can be written as:

$$F_B = g \frac{T_{v,p} - \overline{T}_v}{T_0} \quad (2.5)$$

In equation (2.5), $T_{v,p}$, $\overline{T_v}$ is the virtual temperature of the parcel respectively the environment mean virtual temperature. It is assumed that the parcel's pressure adjusts instantaneously to the environmental pressure. F_B is the buoyant force exerted on the particle. A high virtual temperature of a thermal compared to the environment leads to a positive large buoyant force.

Following equation (2.5), a particle will be decelerated when having a lower virtual temperature than its surroundings, and accelerated when its virtual temperature is higher. Assume that at a certain moment, a particle has a higher virtual temperature than its environment; it starts ascending. In any state of the atmosphere, somewhere the particle will reach the condition where its virtual temperature equals the virtual temperature of the environment.

This height is called the level of neutral buoyancy (LNB). In this level no buoyant force is applied on the particle. If a thermal possesses a vertical velocity at the moment it reaches the LNB, the thermal 'shoots through' this level.

Above the LNB, the parcels potential temperature is lower than the environment, because still the virtual temperature lapse rate of moist air is smaller than that of dry air. From this moment on the parcel is decelerated. If the initial velocity of the particle is too low, it's forced to stop moving upwards. The height this process takes place is called the Convective Inhibition (CIN).

However, the initial vertical velocity at the start of the CIN was high enough, the particle will keep ascending. Still, the particles temperature decreases. Because of the decrease in temperature, the saturation vapor pressure of the parcel decreases. At some point the particle reaches a height at which the vapor pressure equals the saturation vapor pressure.

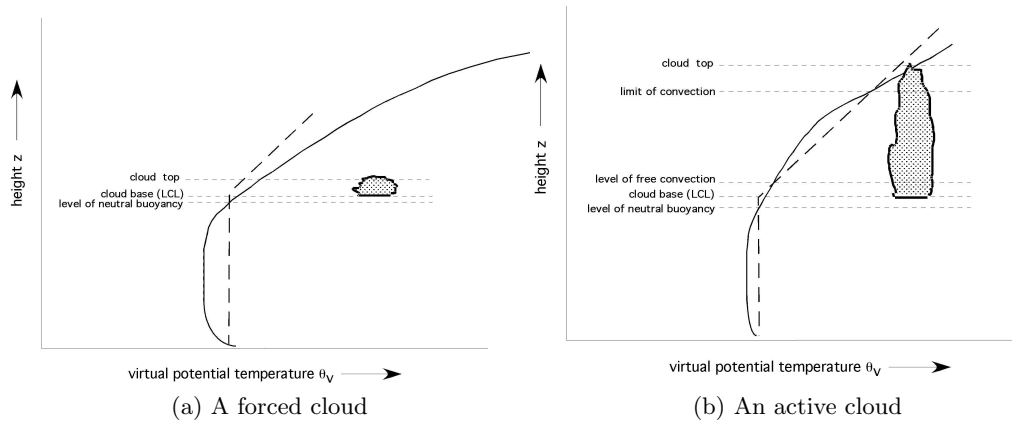


Figure 2.2.2: Schematic views of the most important levels in cumulus formation. The dashed lines represent the virtual potential temperature for an isentropically rising air parcel. The solid line represents the environmental virtual potential temperature. A forced cloud is formed in an absolutely stable atmosphere, while an active cloud an only arise in a conditionally unstable atmosphere. [7]

From this point on, evaporation of water takes place; a cloud is formed. Due to the phase change of the water, virtual potential temperature is not constant with height any more. The parcel will from now on follow the wet adiabatic lapse rate. The heat released due to evaporation may cause the parcel to have a higher temperature than the environment. An important assumption is that the wet-adiabatic lapse rate applies to a parcel that rises adiabatically, without mixing with the environment. Total water content and liquid potential temperature are assumed to remain constant, as explained in section 2.1.5. A schematic figure of the different layers in the atmosphere important for cumulus formation, for active and forced clouds, is found in figure 2.2.2.

A second point of notice is that there are two types of clouds to be named in this context, their formation depending on the change of virtual potential temperature of the environment. If the parcels virtual potential temperature increases slower than the environmental θ_v the parcel will remain heavier than its environment, and therefore finally start descending. The formed cloud is called a forced cloud. A second possibility is that the wet-adiabatic lapse rate of the parcel is higher than that of the environment. In this case, the particle will ascent further until it reaches the so called limit of convection (LOC). Here, the parcel is neutrally buoyant again.

In this higher region of the atmosphere, the same process starts up; again, the parcel will move trough the LOC till it reaches the convective inhibition layer, where it will be forced to a halt if not containing enough initial velocity and/or moist. These processes are however beyond the scope of this project.

2.3 Dutch Atmospheric LES-model

Large Eddy Simulations (LES) are used to numerically simulate the fluid Navier-Stokes equations for incompressible flow. The large scale motions are calculated explicitly, while the small (subgrid) scales are parametrized. An approximation used in this model is the Boussinesq approximation, which leads towards ignoring density variations unless they regard the acceleration of gravity [14]. In an LES model, all different physical processes taking place in fluid dynamics, like radiation and precipitation, are taken into account. In this section, more explanation is given on the specific LES model used for the data evaluation in this report.

The Dutch Atmospheric LES model uses the following equations to describe the atmospheric processes, starting with the conservation equations for:

- the liquid water potential temperature
- total specific humidity
- mass
- momentum

Other processes that are taken into account are radiation, surface fluxes and cloud microphysics [15].

The conservation equation that is solved in an LES model is based on an arbitrary quantity $\Psi \in \{\theta_t, q_t\}$:

$$\frac{\partial \Psi}{\partial t} + u_i \frac{\partial \Psi}{\partial x_i} = -\frac{\partial (u_i'' \Psi'')}{\partial x_i} + S_\psi \quad (2.1)$$

In this equation, u_i is defined via:

$$u_i \frac{\partial \Psi}{\partial x_i} = u \frac{\partial \Psi}{\partial x} + v \frac{\partial \Psi}{\partial y} + w \frac{\partial \Psi}{\partial z} \quad (2.2)$$

S_ψ contains all important processes influencing Ψ , like radiative, chemical or microphysical processes. $u_i \frac{\delta \Psi}{\delta x_i}$ is a term containing the heat flux due to a wind velocity in this direction. $(u_i'' \Psi'')$ denotes the subgrid turbulent fluctuations. These are modelled via:

$$u_i'' \Psi'' = -K \frac{\partial \Psi}{\partial x_i} \quad (2.3)$$

In equation 2.3, K is the eddy diffusivity constant. The calculation of K is beyond the scope of this project [16].

The research data is gained as explained in the introduction and modelled by J.J. van der Dussen as shortly explained above.

2.4 Mathematical Tools

2.4.1 Autocorrelation

A way to depict the correlation of a variable with itself over time is by calculating its autocorrelation. This function quantifies the amount of common variation between the variable at time t and that same variable at a later time $(t + \tau)$, in which τ is the time between the compared samples. An autocorrelation of 1 indicates perfect correlation of a wave or signal with itself, -1 indicates perfect anti-correlation and 0 means no significant correlation is shown. In other words, autocorrelation is a tool to calculate the persistence of a signal over its whole duration time [17].

The autocorrelation can be calculated for different time lags n_τ , defined via $\tau \equiv \Delta t \cdot n_\tau$. In this definition, Δt is a variable time step. The final autocorrelation function $\rho(\tau)$ gives insight in the timescales for which a signal is persistent. A persistent signal therefore would confirm a persistent structure, while finding a zero-correlated signal indicates turbulent structures.

The autocorrelation of a discrete function $A(k)$ can be written as [17]:

$$\rho(n_\tau) = \frac{\sum_{k=0}^{N-n_\tau-1} [(A_k - \overline{A_k}) (A_{k+n_\tau} - \overline{A_{k+n_\tau}})]}{\left[\sum_{k=0}^{N-n_\tau-1} (A_k - \overline{A_k})^2 \right]^{\frac{1}{2}} \left[\sum_{k=0}^{N-n_\tau-1} (A_{k+n_\tau} - \overline{A_{k+n_\tau}})^2 \right]^{\frac{1}{2}}} \quad (2.1)$$

To rewrite $\rho(n_\tau)$ to a function of the time lag, following relation is used:

$$\rho(\tau) = \Delta t \cdot \rho(n_\tau) \quad (2.2)$$

The averaged values indicated by overbars are time averages:

$$\overline{A_{k+n_\tau}} = \frac{1}{N - n_\tau} \sum_{k=0}^{N-n_\tau-1} A_{k+n_\tau} \quad (2.3)$$

The time average A_k follows from 2.3 with $n_\tau = 0$. N is the total number of time steps taken. The discrete variable k is defined as $t \equiv \Delta t \cdot k$.

Definition of the mean

In the approach described above, the mean value that is calculated changes with the timestep n_τ . If $n_\tau = 0$, the average $\overline{A_k}$ of variable A is an average over the first N steps; over the whole selected measurement time. While as $n_\tau = n_{\tau_{max}} = N/2$, A_k is only averaged over the first half of the time series. Of course, the number of elements used to calculate the average A_{k+n_τ} also changes with n_τ . This means that for each step n_τ , the average changes, while the average is used as a reference, in fact only the change compared to this particular average is taken into account. In an alternative autocorrelation the average is constant and taken over the whole data series, $A_k + n_\tau$ is defined as:

$$\overline{A_{k+n_\tau}} = \frac{1}{N - n_{\tau_{max}}} \sum_{k=0}^{N-n_{\tau_{max}}-1} A_{k+n_{\tau_{max}}} \quad (2.4)$$

In this equation, $n_{\tau_{max}} = N/2$. To check this alternative approach, both $\overline{A_k}$ and $\overline{A_{k+n_{\tau_{max}}}}$ can be filled in equation 2.1. This results for into $\rho(n_{\tau=0}) = 1$.

2.4.2 Integral timescale

The integral timescale is a measure of the longest connection or correlation of two points. If the autocorrelation $\rho(\tau)$ of a variable is calculated for a range of values of τ , the integral timescale can be calculated by integrating $\rho(\tau)$ over τ .

$$\tau_{int} = \int_0^{t_{end}} \rho(\tau) d\tau = \sum_{t=0}^{n_{end}} \rho(n_\tau) \Delta t \quad (2.5)$$

This integration can be executed in four different ways [18], the difference between the four approaches is the upper integral boundary t_{end} . First option is to integrate over the whole domain of τ . Another option is to integrate up to the value where the autocorrelation function is a minimum, if the autocorrelation has a negative region. The third and fourth options both integrate to a point where the value of $\rho(\tau)$ equals $1/e$ respectively 0. In this report, the upper summation limit n_0 is defined as the first point where the autocorrelation is equal to zero. The reason for this choice is based on measurements done by O'Neill et al. [18] on autocorrelation functions applied to models that use periodic boundary conditions. In this article the investigated variable was length, while we are calculating the integral timescale. The difference between length and time is a simple multiplication with the mean velocity, which does not influence the integration limits or final result.

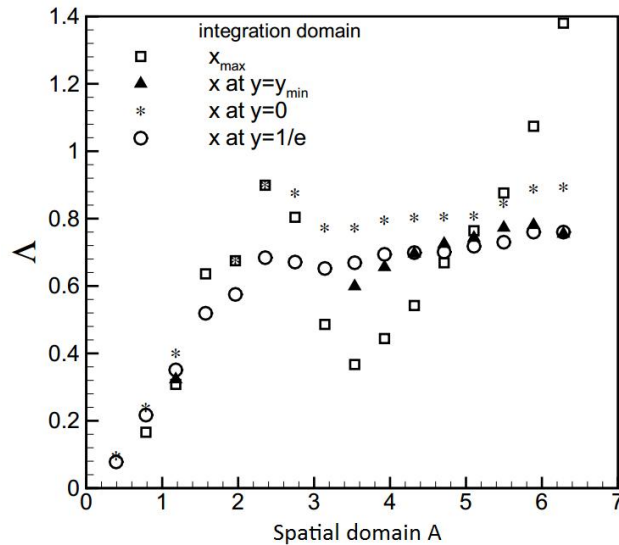


Figure 2.4.1: Integral length (Λ) against the used spatial domain, plotted for four different upper integration limits. Graph copied after O'Neill et al. [18]. Note the strong influence of the spatial domain on integral lengthscale calculated using the maximum value in the domain as upper integration limit.

O'Neill found that integrating over the whole time domain gave an abusive integral scale, because of the periodic boundary conditions in an LES model. Integrating up to the minimum autocorrelation is not always possible; sometimes the autocorrelation function does not reach minimum within the domain that is used. Integrating is expected to underestimate the integral time scale. Therefore the upper integration limit is chosen as

the first zero crossing of the function. In some exceptional points, the autocorrelation does not reach zero within the domain of τ of two hours. The upper limit of the integral is theoretically undefined. The integral time scale is then calculated by integrating the autocorrelation over τ to the maximum value of τ ; which is 2 hours. Since discrete values have been used, the final integral time scale is calculated via:

$$\tau_{int} = \sum_{n_{\tau=0}}^{n_0} \rho(n_{\tau}) \cdot \Delta t \quad (2.6)$$

In this equation n_0 represents the chosen upper integration limit; the first point where the autocorrelation equals zero. $n_{\tau=0}$ represents the first step.

Chapter 3

Setup

3.1 LES domain

The domain of the simulations has 128 grid points in x and y directions, each having a spacing of 35m. In the vertical dimension, the resolution varies with height, because a high resolution at the top of the boundary layer is required. For the first 400m from earth surface a spacing of 15 m is used, from that height on this spacing is gradually decreased to a spacing of 5m per grid step. The total domain size is thus 4462.5m x 4462.5m x 2175.8m (x, y, z). The model domain has a velocity of with -2 and -7 ms^{-1} in respectively the x and y direction relative to the earth based measurements. This model velocity is used to minimize numerical errors [4, 19].

From the two consecutive days of measurements in the ASTEX case starting 12 june at 17.19 UTC, only the hours 29-32 are considered. This means, actual time of the measurements was at 22.19-01.19, at 13-14 june.

3.2 Considerations

3.2.1 Cloud base and top

From the 3D-data fields it appeared that a mean liquid water content of about 0.3 gkg^{-1} was found between 1.4km and 1.8km, probably this shows the thinning stratocumulus layer. Cumulus cloud base is located at a height of 500-600m, the shallow cumuli in this domain have a typical height of 1km.

3.2.2 Life time of a cloud

The characteristic lifetime T of a cloud is estimated in terms of its height H and vertical velocity w_* via:

$$T = \frac{H}{w_*} \quad (3.1)$$

In equation (3.1), w_* is the characteristic vertical velocity scale, based on the vertical integral of the buoyancy flux. w_* has an approximate value of 0.6 - 1 ms^{-1} . The height of shallow cumulus can be approximated with 1km. Therefore the lifetime of these clouds is estimated to be in the order of 20-30 minutes. This is confirmed by visual inspection of the fields. In observations made during ASTEX, the lifetime of a cloud was one hour.

3.2.3 Lagrangian translation of the 3D field

In this project, the purpose is to analyse correlations between locations representing (approximately) the same air. Therefore, the air mass is followed as it moves with the horizontal mean wind.

The velocity in the 3D fields is not the real velocity, but the velocity in respect of the DALES model translation velocity. This translation velocities of -2 and -7 ms^{-1} are optimized for the whole series of ASTEX measurements. Therefore, the air mass in the data environment still has a horizontal velocity. Note that with data environment the 3D data fields produced by the DALES model are meant.

In order to get a good view on correlations in the same air mass, it is necessary to move with the same velocity as the air mass. This is done by calculating the mean velocities in West-East and South-North (x and y) directions. These velocities are denoted as u and v respectively. Each time step, the average is taken over the 3D grid, where only data points higher than 900m are taken into account.

This results into the following velocities: u starts at a value of -1.85ms^{-1} , and increases linearly with time to its final value of -1.3ms^{-1} . The change in v is even bigger and also linear with time: from 2.5 to 4.5ms^{-1} . Each time step the data will thus be translated with a different velocity in x and y direction. In formula the translated location x'_n of frame n is expressed as a function of its original location x_n , translated with the total of the displacements between each frame.

$$x'_n = x_n - \Delta t \cdot \sum_{i=1}^n u_i \quad (3.2)$$

In this equation u_i represents the velocity in the x direction at time i . In the y direction, the same formula can be applied.

After this data processing, a visual inspection of a surface plot of the liquid water path is used to check if the translation velocity equals the velocity of the air mass. This will not be shown in the report, although material is available. For the remainder of this report, all variables are evaluated in a reference frame that moves with the same mean velocity as the air mass does.

3.3 Rough approach

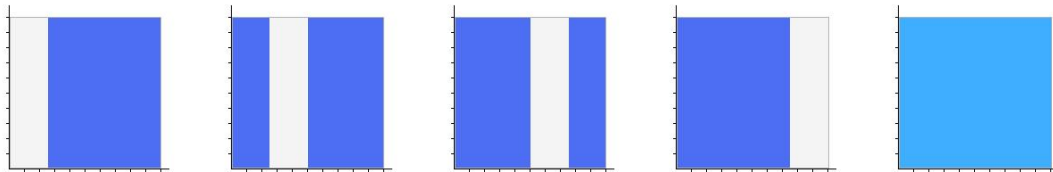
3.3.1 Cloud presence

A basic check to evaluate the shallow cumulus clouds and their persistence is by calculating how often a certain liquid water path is found in each column. In formula, the cloud presence c_t can be expressed as follows:

$$c_t(x, y) = \frac{\sum I_c(x, y)}{\sum I(x, y)} \quad (3.1)$$

In which I_c represents 1 if $W > W_{min}$, and 0 if this is false. I is each time frame equal to 1; its sum averages the result. This means $c_t=1$ at a position a cloud is during the whole measurement time, and $c_t=0$ if no cloud is present at all during the measurement time. If the cloud presence is perfectly random, the time mean cloud presence \bar{c}_t equals the average cloud fraction c_f .

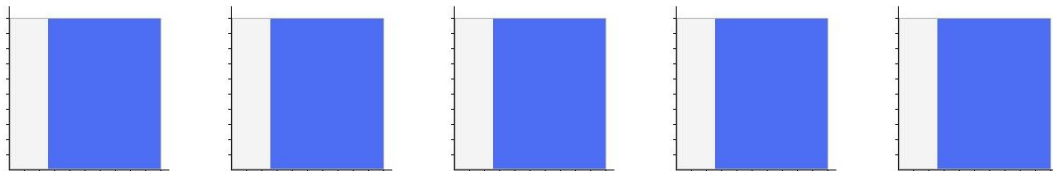
The principle of this method can be explained by a simple schematic example in figure 3.3.1. In this example, the total amount of liquid water is constant. The location of the moist is different to visualize the meaning of cloud fraction. Assume we have a square region, in which the a quarter is cloud during the first time step. In the second time step, the cloud is moved a to the right, or it stays where it was. In four time steps, following figure is a schematic drawing of how these two extremes develop. The time step in this explanation is arbitrary, therefore no units are given.



(a) first time step (b) second time step (c) third time step (d) fourth time step (e) total time

Figure 3.3.1: Figures of the cloud presence change during time. Figure 3.3.1e represents the overall cloud presence in case of a 'random' process.

As is depicted by the figures, the overall fraction of time a cumulus cloud is present strongly on how persistent or repetitious a signal is; the first series shows no overlap between the four consecutive time steps, resulting in an overall homogeneous cloud presence of 0.25. In a second series of measurements, the cloud stays at the same location. Shown in figure 3.3.2



(a) first time step (b) second time step (c) third time step (d) fourth time step (e) total time

Figure 3.3.2: Figures of the cloud presence change during time with a theoretical perfect persistent cloud. Figure 3.3.2e represents the overall cloud presence.

Maximum total cloud presence is now found in the persistent part of the figure and equals 1, minimum is 0. The average cloud presence over the whole area is still 0.25, as it defined.

A cloud is selected to have a liquid water path of at least 0.1 kgm^{-2} . This value is chosen to select cumulus and ignore the stratocumulus that typically has a smaller liquid water path. With a surface plot, the cloud presence of the total measurement time is shown for the evaluated area.

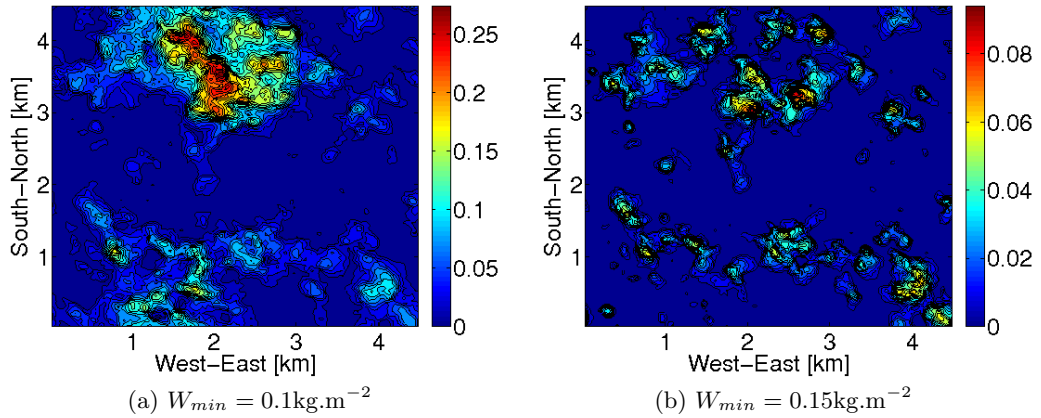


Figure 3.3.3: The average fraction in figure 3.3.3a was 0.0362. This fraction is the fraction of the total time a cloud was present with a $W > W_{min}$. In figure 3.3.3b the average fraction was 0.0074. A fraction of 0.27 thus means that over the whole measurement time of four hours, the accumulated time a cloud was present at that point is more than one hour. Note that this is the accumulated time, it does not say much about the consecutive time clouds were present.

As explained in the caption of figure 3.3.3, the accumulated time of cloud existence located at the red contours in the figure is one hour. This is longer than the expected time if the clouds would be distributed perfectly random with time. Above that the maximum cloud cover is significantly larger than the average cloud cover (a maximum of 0.29 against an average of 0.0362). Conclusions however should not be drawn too quick, since the presence of the stratocumulus could still be measured in the cloud cover. In order to be absolutely sure of excluding the stratocumulus layer, the same method can be applied to the specific liquid water content at different heights. This results in the cloud fraction.

3.3.2 Cloud fraction

The cloud fraction is another way to depict how often a minimum specific liquid water content $q_{l,min}$ is found. Three representative heights are 600m, 1000m and 1500m.

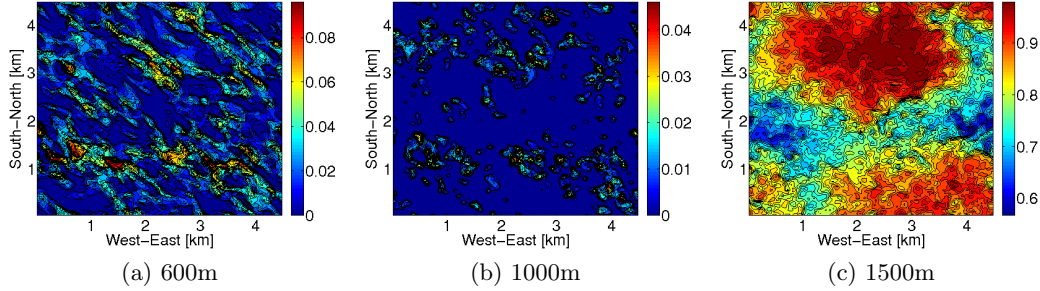


Figure 3.3.4: Cloud fraction surface plots at two different heights. It can be seen that the most persuasive pattern is found at a height of 1500m, where also the thinning stratocumulus is located. In these figures, clouds are defined to have a specific liquid water content of 0.05 gkg^{-1}

From these results, it is already visible that the stratocumulus layer has a very large fraction. Lowering the minimum specific liquid water content for a cloud to 0.5 mgkg^{-1} does not change the images nor cloud fraction significantly. It would therefore be interesting to investigate the vertical correlation of this particular cloud layer, to gain more insight on how this probably persistent structures are originated.

3.4 Time averaging

3.4.1 Expectations

Cumulus clouds are formed via a random turbulent process. Therefore a surface plot of the liquid water path averaged in time over the whole measurement series, should result into a random structure with small values of W compared to the normal liquid water path in a cloud of about 0.1 gkg^{-1} . In order to visualise the development of this average, four timeslots are used to calculate the hourly averaged profiles. After that, the time average over 4 hours is calculated for the same surface. This has been done for the variables W , q_t , q_r , θ and w . In this section, all figures of W will be shown as an illustration. The development of the averaged profiles of the other variables can be found in appendix A, for them, only the averaged profile over total measurement time is shown.

Liquid water path

Liquid water path is the specific liquid water content integrated over height (see eq. 2.3). Therefore, W of these 3D fields is already a 2D surface. The results of the different averaged hours can be seen in following figures;

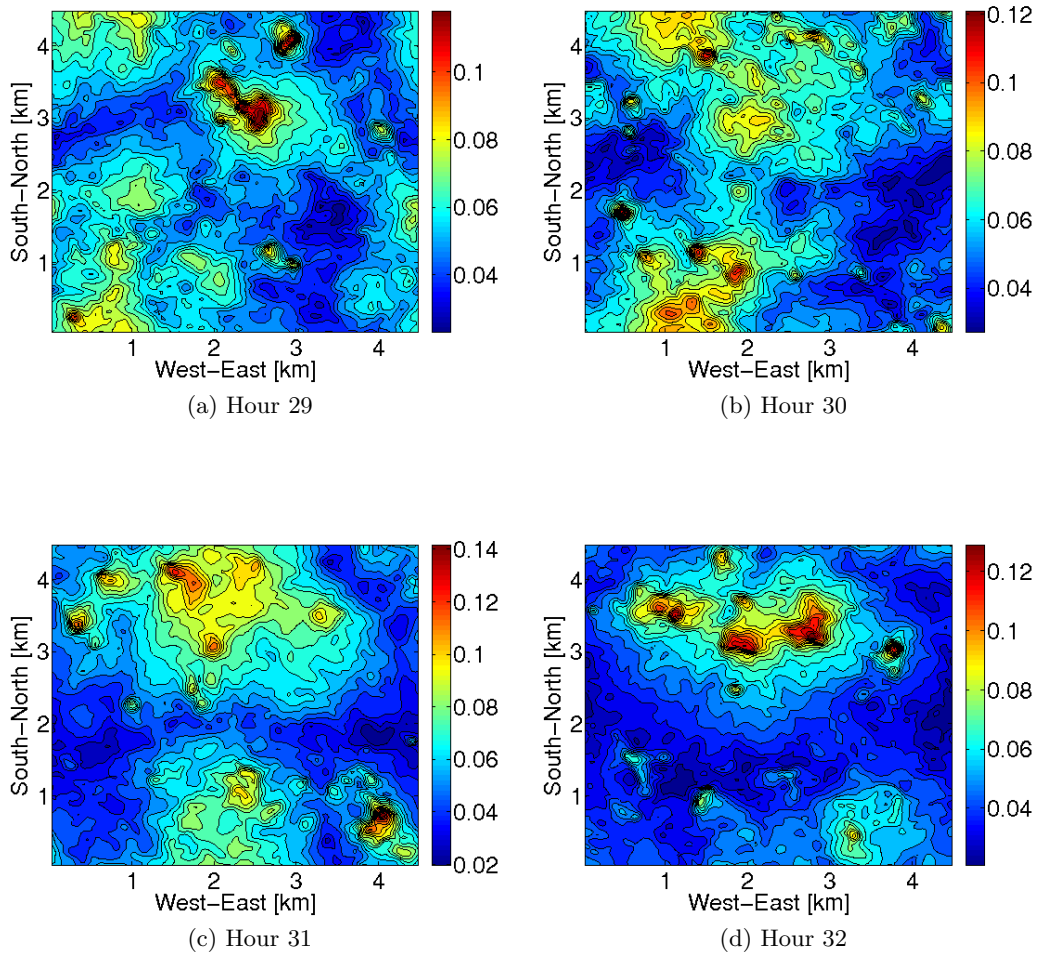


Figure 3.4.1: Liquid water path averaged in time for four different timesteps, split in hours 29-32 of the ASTEX measurements.

The lifetime of a cloud is estimated to be in the order of half an hour. This means that a persistent cloud (existing for ≈ 45 min) can maximally overlap two consecutive figures. This could explain the similarity of two consecutive hours. But there is also a similarity shown between the figure of hour 29 and hour 32. This pattern can also be seen in the total time average:

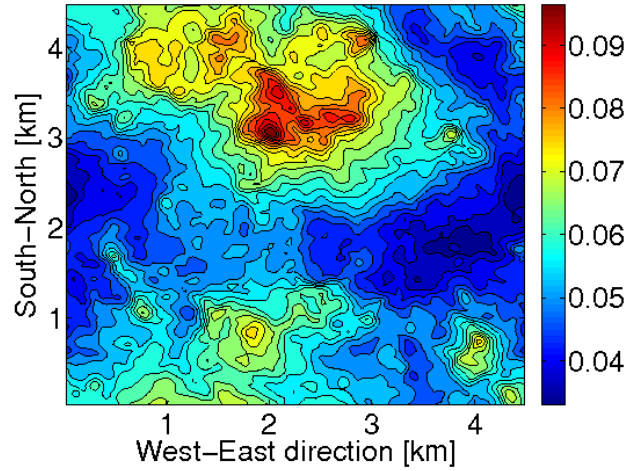
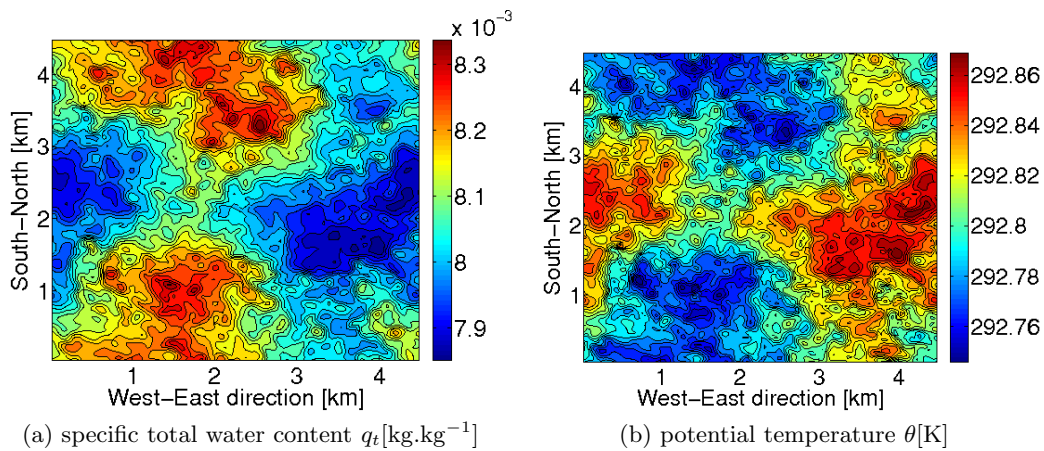


Figure 3.4.2: Averaged liquid water path over total measurement time [$\text{kg}\cdot\text{m}^{-2}$]

Evaluating the figures of the time averaged liquid water path, the presumption that clouds are more or less persistent is somewhat confirmed by these figures. The other variables show a comparable result.

Other variables

The other variables are evaluated in the same way as has been done for the liquid water path, with this difference that the time average is calculated at a height of 1km for each variable. For completeness, the hourly averaged surfaces can be found in appendix A. In this section, only the time averages over total measuring time are shown. Expectation of these results is that most variables show a correlation or anticorrelation with the time-averaged liquid water path. An extra check to exclude the stratocumulus layer is made by adding a 'new' variable; the total water path. This is in fact almost the same as the liquid water path, but instead of integrating q_l over the height of the grid column, q_t is integrated.



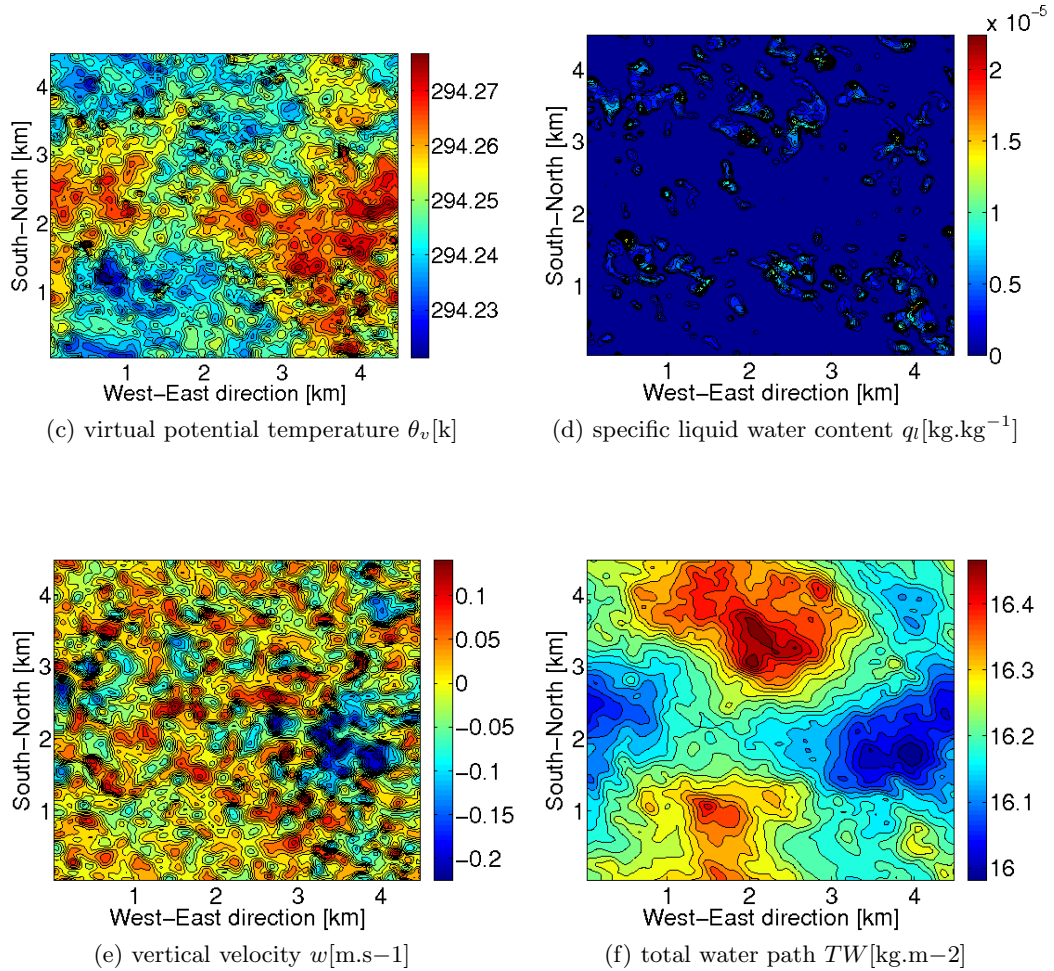


Figure 3.4.3: Variables shown in these plots are averaged over total measurement time (hour 29 to 32), at a height of 1km. Except for the total water path (TWP) since this is a vertical integrated value.

3.4.2 Evaluation

As can be seen in the compilation of figures 3.4.3; there are visible accumulations of high or low values of a specific variable over time at certain points. For the vertical velocity w probably most fluctuations are expected to be caused by turbulence. This is not absolutely true; although the overall average of the vertical velocity is zero, variations are not that small, there are some points where the average over four hours of measurements equals -0.2 m.s^{-1} , where the non-averaged vertical velocity varied between -0.5 and 0.5 m.s^{-1} . This indicates persistent downdrafts, found at points where least vapor is found.

Another interesting result from these plots is the strong anti-correlation between the total specific water content and the potential temperature, although the order of changes in the potential temperature is very small; variations in (virtual) potential temperature are in the range of 1K, averaged profiles have variations of 0.1K. The potential temperature and specific total water content also look like the profiles of θ and W .

If changes in a variable are completely random, their resulting average over time should equal zero. This also explains that the variations of the averages should at least show a decrease in order comparing them with a non-averaged signal. In contrast, the averaged profile of the liquid water stays in the same order as the non-averaged signal per time step. In the averaged plot a maximum of approximately 0.1 kg.m^{-2} is found against variations of 0.2 kg.m^{-2} of the original signal. This indicates a persistent structure, which is further investigated in this report. The mean variations of q_t, q_r, θ and θ_v are approximately one tenth of the original signals. A comparable result is also found at a height of 600m.

3.5 Summary and look ahead

Summarized, this chapter gives a nice draft on the possible persistence of shallow cumulus. This is based on the cloud fraction, cloud cover and the time averages. But it would be nice to use a more reliable tool to numerically evaluate the time scale of the persistence, and compare this with the expected lifetime of the clouds. A useful tool in this case could be the autocorrelation, and the integral length scale.

It appeared that the persistent 'cloud' as been found in the time-averages of the liquid water path is also found at a height of 1500 in the stratocumulus layer, as seen in section 3.3.2. This could indicate two things; it could be that the persistence that is found is caused by the stratocumulus layer. The average liquid water content of the stratocumulus however is significantly smaller than the liquid water content of the shallow cumuli. A second possibility is that there are vertical correlations between the stratocumulus and the shallow cumuli.

Next to the persistence that seems to be present, a strong anti-correlation between q_t and θ is seen. This anti-correlation will be further investigated in ???. In this appendix, we are looking for the theoretical explanation of this result.

Chapter 4

Autocorrelation

4.1 Introduction

The exact parameters of the autocorrelation calculations as explained in section 2.4.1 are $N = 476$ time steps n_τ , with a size of each time step Δt of 30s. The autocorrelation function $\rho(\tau)$ can be calculated at every grid point (x, y, z) of the dataset. To reduce computational time the integral time scale is calculated at one third of the grid points. This will influence the final resolution of the surface plots. The value n_τ is varied from $n_\tau = 0$ to $n_\tau = \frac{N}{2}$ or the closest smaller integer.

Based on observations in the previous chapter, three different points are chosen to be evaluated further. Point A is located at the highest time average of the liquid water path, found around 2.5km East and 3.4km North (see figure 3.4.2, as observed in our domain that moves along with the air. Point B is located at 1km East and 1.2km North and represents an intermediate of the lowest and highest values of the liquid water path. Then finally point C is located where the downdrafts are observed in figure 3.4.3e; at 3.5km East and 1.9km North. As seen from above, the locations of the three points is shown in figure 4.1.1 and table 4.1.

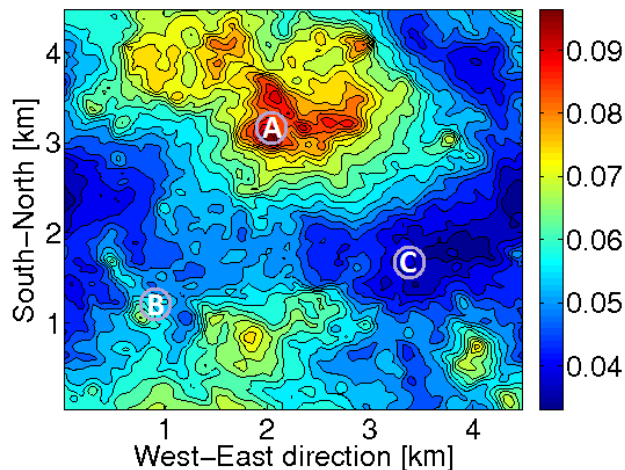


Figure 4.1.1: Locations of the three different points that will be used to visualize the calculation of the autocorrelation and integral time scale. The locations are shown on the total time averaged liquid water path, to visualise the choice of the different locations.

Table 4.1: Locations of the points A, B and C

Point	West-East	South-North
A	2.5km	3.4km
B	1km	1.2km
C	3.5km	1.9km

4.2 Expectations

The autocorrelation can be calculated to gain knowledge on the persistence of a certain signal, or in this case, different variables. Therefore it is a helpful tool to test our hypothesis that clouds are returning or arise at (nearly) the same place. Therefore the autocorrelation of different important variables for the formation of a cloud should result in a larger time scale than the typical lifetime of the clouds. This typical lifetime is based on both an order estimation and visual inspection of the shallow cumulus fields. Based on the previous chapter, it is expected that the autocorrelation is high at the points where a high time average of the liquid water path was found.

After checking the autocorrelation at the specific points A, B and C, surface plots of the integral time scale will be compared to the time-averaged surface plots made at the same height of the same variable. It is expected that these figures give a pattern that agrees with previous results and a maximum integral time scale larger than the approximated life time of the clouds of 30 minutes.

4.3 Linear trend of the variables

In the four hour duration of the simulation, the different variables could have a (linear) trend in the same order as the variations of the signal. If a variable has a linear trend, the autocorrelation would return a misleading high value. A linear trend results into equal positive or negative change of a property, and thus a (false) high autocorrelation since we were looking for correlations in the fluctuations of a variable, not the trend. To check whether the evaluated variables have a significant trend, each time step the slab mean is calculated at a specific height (600m 1000m 1300m and 1500m). As an example, the result of one of these calculations is shown in following figure for the virtual potential temperature at a height of 600m.

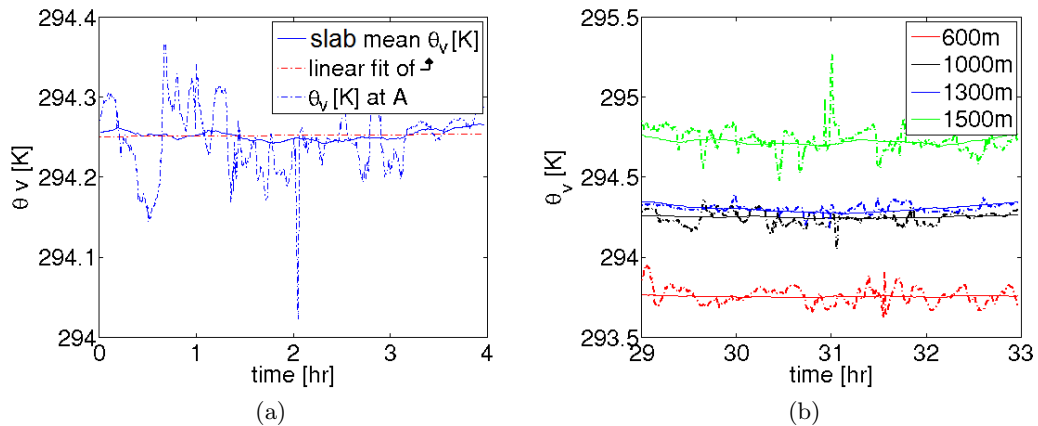


Figure 4.3.1: 4.3.1a: Variation in time of the virtual potential temperature at one specific point compared to the evaluation of its slab mean value. The linearization of the slab mean value is shown with a dotted line in the graph. Figure 4.3.1b shows the potential temperature after correcting it for its linear trend, plotted for four different heights. In this figure slab mean is plotted in a solid line, while a single point is plotted with the dashed line.

The linear trend appeared to be significant for the liquid water path, potential temperature and virtual potential temperature. For completeness, all variables are first corrected for their own trend, even if this trend was negligibly small. A final check if this correction has the expected effect is done by checking the slab-average change in time after the correction is applied.

4.4 Autocorrelation and integral timescale

The autocorrelation of different variables ($w, \theta_v, \theta, q_t, W$ and q_r) is calculated in two ways, described in section 2.4.1. The first calculation is the one presented by Stull [20] and an alternative autocorrelation that uses not a varying average, but one that is the same for each time step. In following graphs, both ways of calculating the autocorrelation are shown; the alternative with a dotted line, and the primary function of Stull with a solid line. The locations of point A, B and C can be found in table 4.1 and figure 4.1.1.

The integral time scale is calculated as written in equation 2.5, and used to relate autocorrelation with the lifetime of the clouds. This time scale however is not a uniform time scale; different approaches are known. In this section, the integral time scale is calculated by integrating the autocorrelation in τ till the value of the autocorrelation reaches zero. This is done for each grid point for which the autocorrelation is calculated. To illustrate this approach, the integral time scale at one point is plotted next to the autocorrelation at that specific point.

Note on the figures

In both the autocorrelation and integral time scale figures the dash-dot line represents the alternative autocorrelation, and the solid line the one presented by Stull. In the figures on the integral timescale, a solid line for Stull's function becomes a dashed line at the point autocorrelation crosses zero for the first time. For the alternative autocorrelation a das-dotted line becomes a dotted line at the point its corresponding autocorrelation is zero.

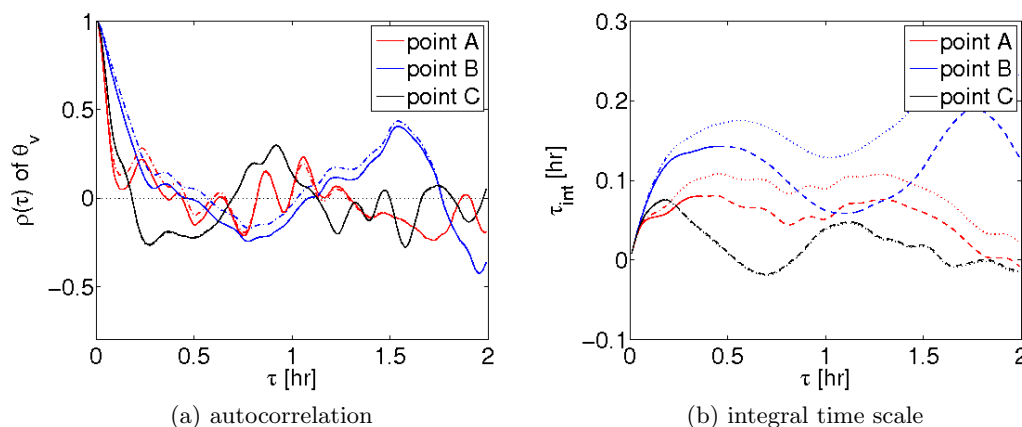
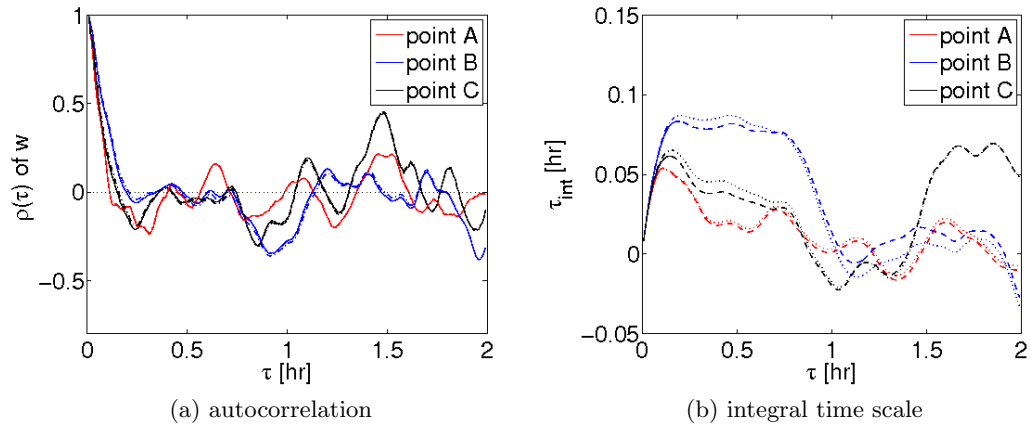
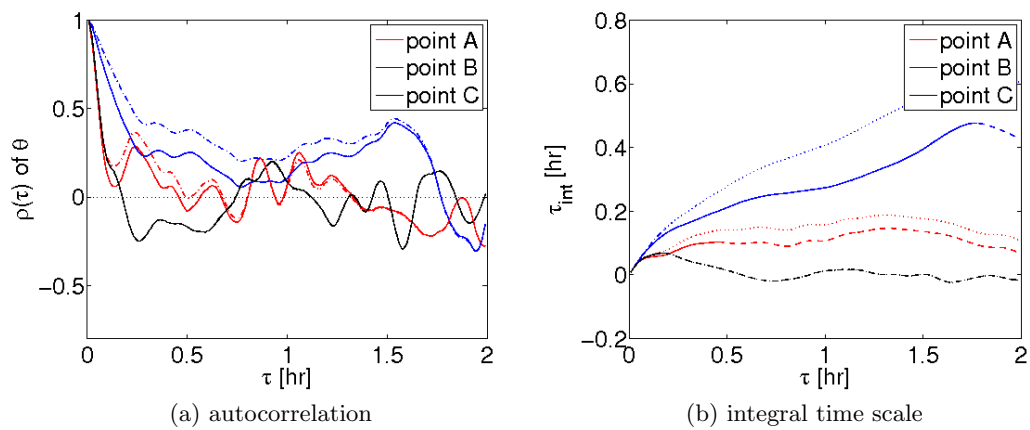
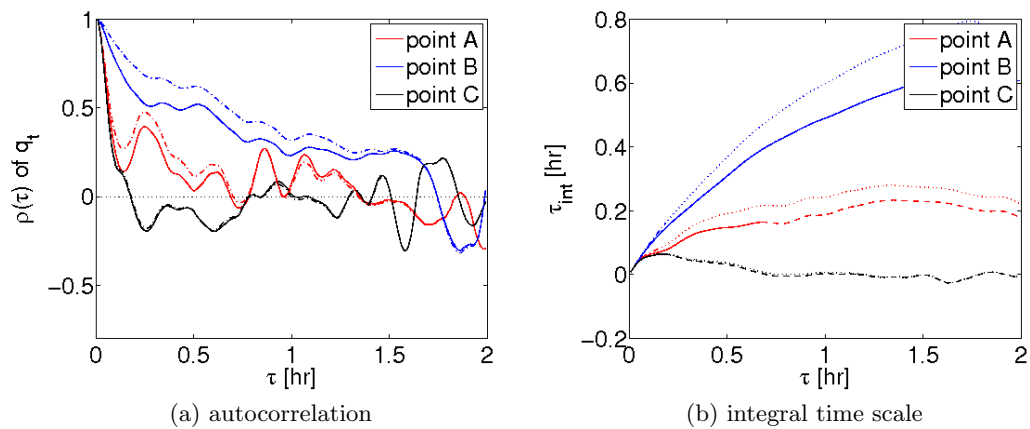
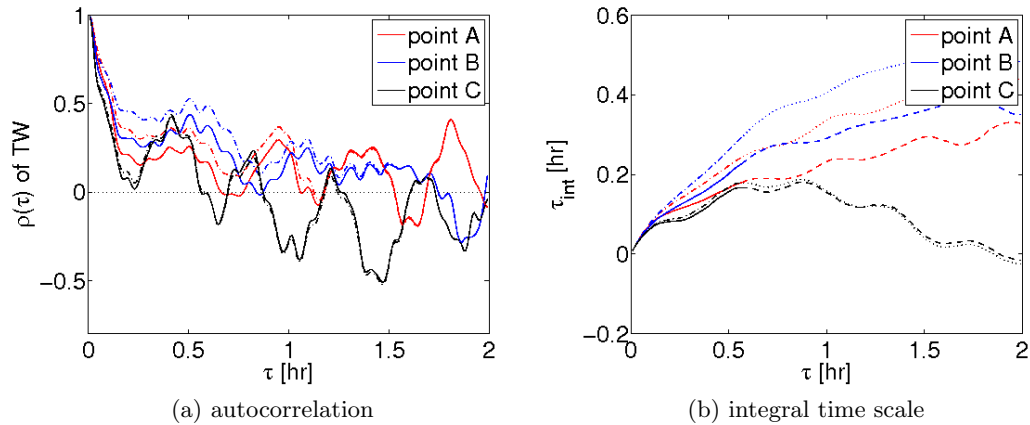
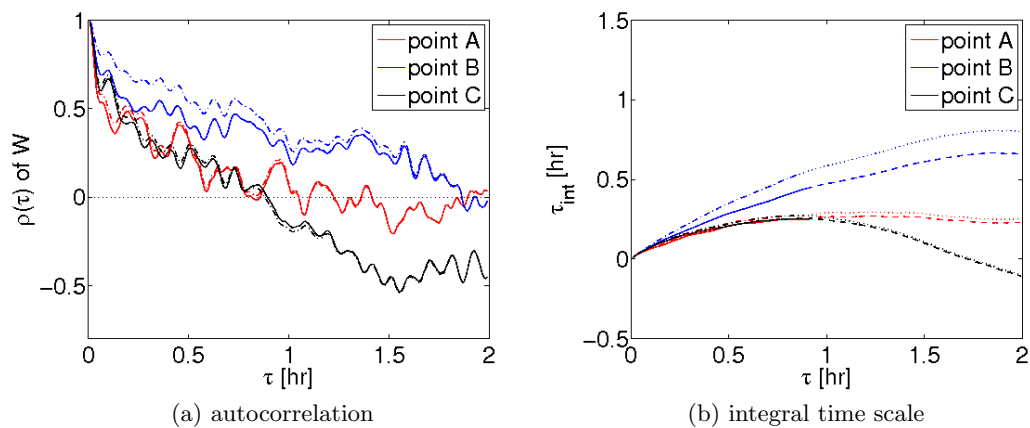


Figure 4.4.1: Virtual potential temperature θ_v

Figure 4.4.2: Vertical velocity w Figure 4.4.3: Potential temperature θ Figure 4.4.4: Specific total water content q_t

Figure 4.4.5: Total water path TW Figure 4.4.6: Liquid water path W

Integral time scale

At the moment the solid line of the integral time scale becomes dotted in the figures, the autocorrelation has reached its first zero. The final integral time scale for the different variables at 1km height varies between 6 minutes and 43 minutes. Lowest integral time scales are found for virtual potential temperature and vertical velocity, the time scales of these variables are not bigger than ± 6 minutes. Total water content shows the highest integral time scale. These figures however only show three selected points. In the following section, a better view on the integral time scale is given using surface plots. These figures already indicate something about the autocorrelation at the three different points.

Comparing points A, B and C

Following the results of the previous chapter, the most persistent cloud seemed to be located at point A. But the autocorrelation and integral time scale at point B appeared

to be higher at point B than at point A. As expected, the autocorrelations where least clouds, and an average downdraft was found (point C) is lowest, except for the vertical velocity and virtual potential temperature. Especially the vertical velocity has a very small integral time scale of about 6 minutes, and the difference between the three points is within three minutes from each other.

Stull v.s. alternative

Another point we can make up from these results is that the autocorrelation as given by Stull, and the alternative approach using a constant average do not differ significantly, although the alternative approach results in a higher autocorrelation than Stull's. In the remainder of this report, Stull's autocorrelation function is used.

Fluctuations

The autocorrelation shows strong fluctuations, which are not shown in other articles using autocorrelation to investigate persistent structures in fluid dynamics.

4.4.1 Integral time scale surface plots

As has been done in preceding figures for one point, the integral time scale for one third of the grid points of the dataset is calculated at a height of 1000m and 600m. The results for this integral time scale are shown in a surface plot. Plots are compared with the time averaged surfaces presented in section 3.4. For completeness, these figures are shown again next to the integral time scale surfaces.

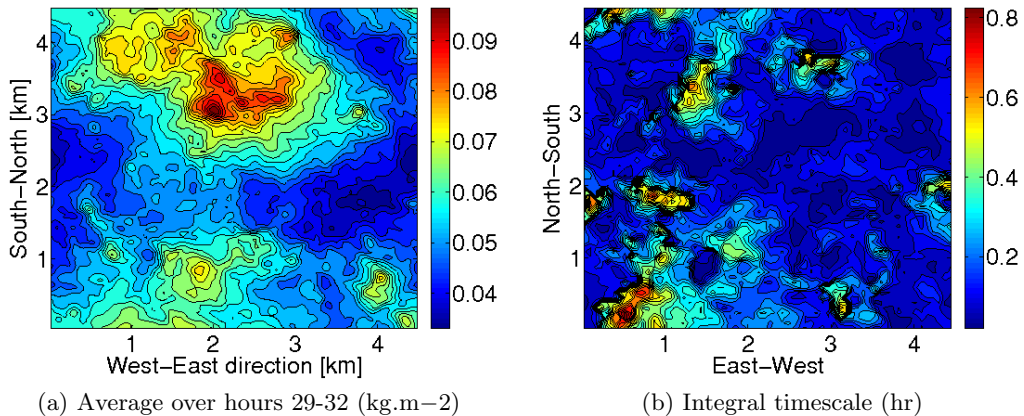
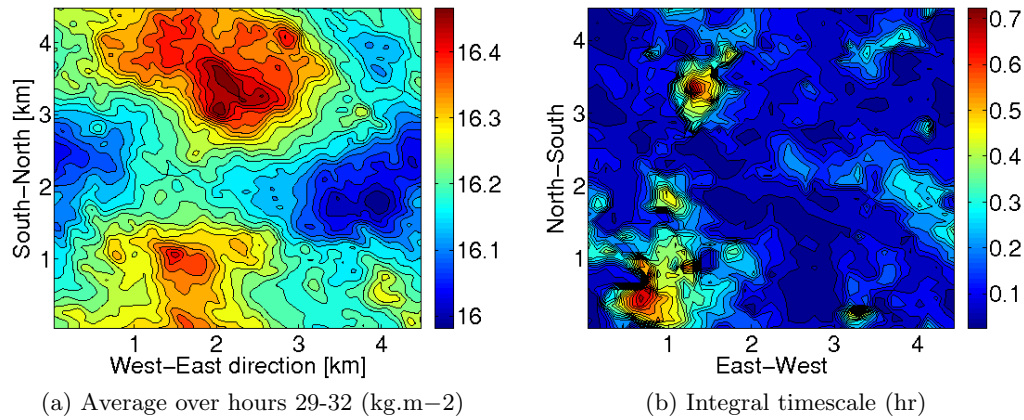
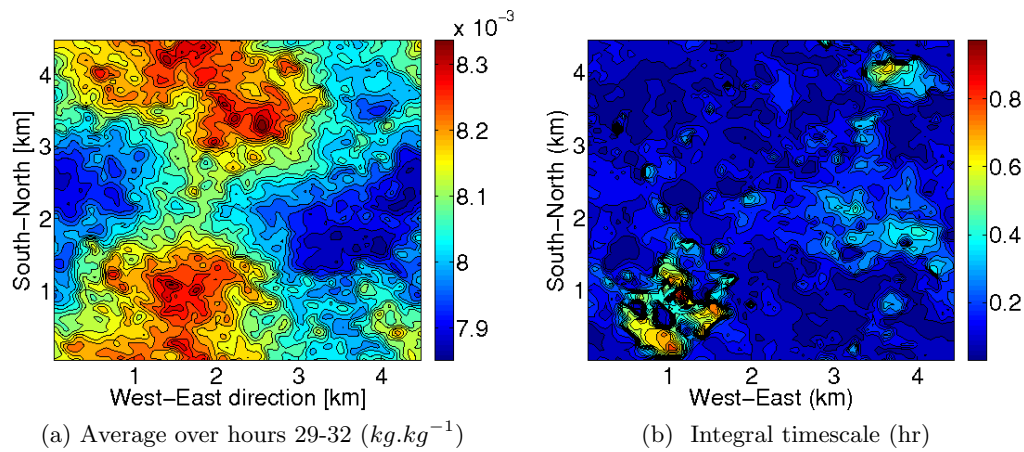


Figure 4.4.7: Liquid water path W .

The liquid water path averaged over the hours 29 till 30 next to the integral time scale surface plot. The maximum integral timescale of about 0.75 does show that a correlation bigger than the typical lifetime of a cloud is found at some points.

Figure 4.4.8: Total water path TW .

The total water path averaged over the hours 29 till 30 next to the integral time scale surface plot. As seen for W , also TW shows agreements between the averaged profile and the integral time scale profile. Most agreement is found in the North-East of the figure.

Figure 4.4.9: Specific total water content q_t at a height of 1km.

The integral time scale for the total specific total water content reaches 0.9 hour at its top. At a height of 600m, the maximum timescale is 0.3 hour.

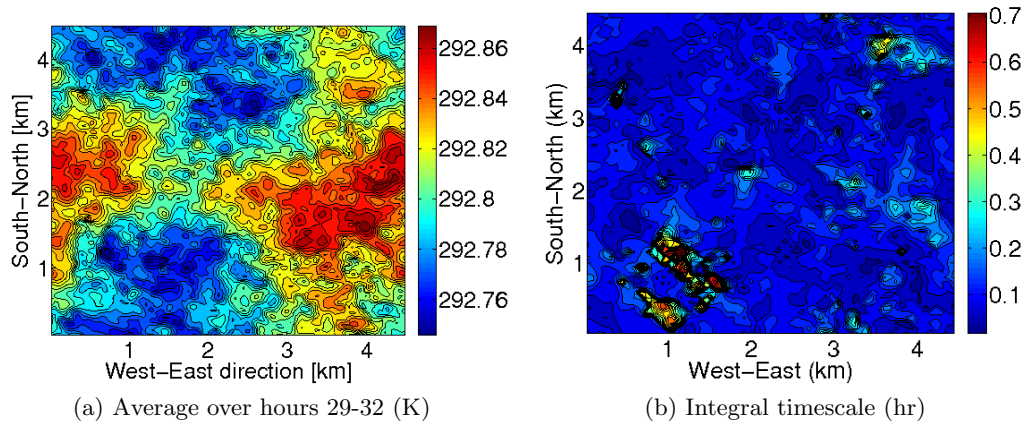


Figure 4.4.10: Potential temperature θ at a height of 1km.

The integral time scale of the potential temperature shows a similarity with its time-averaged figure. Note the correspondence in the integral time scale of θ and q_t . At a height of 600m a small similarity is seen as well, but the integral time scale reaches a maximum of only 0.22 hour.

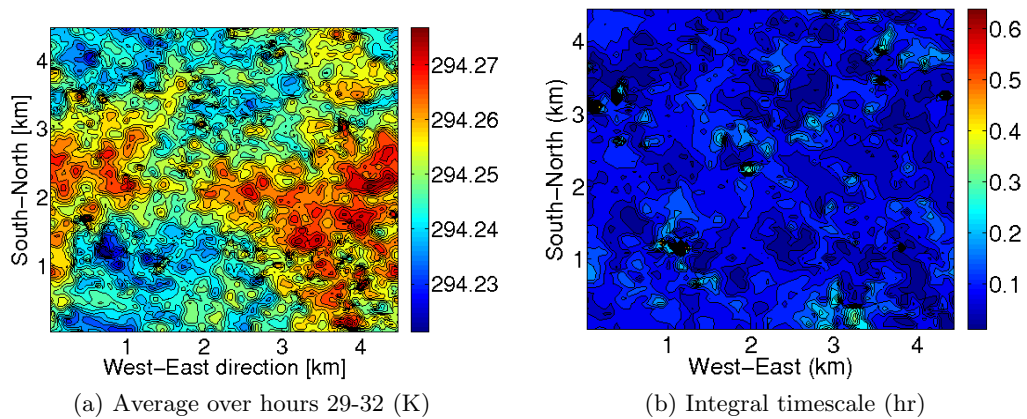


Figure 4.4.11: Virtual potential temperature θ_v at a height of 1km.

The integral timescale of the virtual potential temperature does not correspond to the average over the hours looking at the figures above. At a height of 600m, the integral timescale has a maximum of about 0.22 hour, in contrast the pattern of the average contourplot shows more similarity with the integral timescale contourplot.

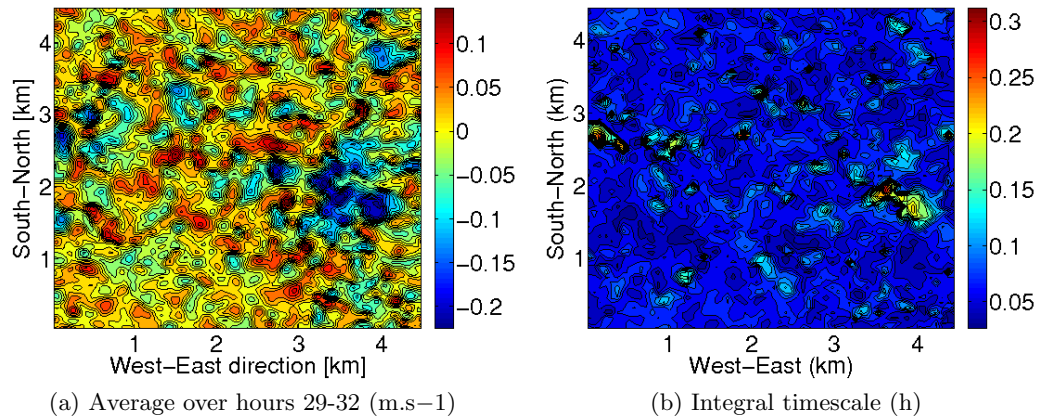


Figure 4.4.12: Vertical velocity w at a height of 1km.

The vertical velocity does show a stronger autocorrelation at the locations where the downdrafts are found. These figures are made at a height of 1000m. At 600m height, these downdrafts are less evident, which is also seen in the autocorrelation surface plot; at 600m the maximum autocorrelation is 0.1 hour.

4.5 Summarized results

The autocorrelation as presented by Stull shows lower integral time scales, and is therefore chosen in order not to overestimate the actual integral time scale. Following Treberth [21], this specific autocorrelation calculation even gives an underestimation of the true integral time scale. This could be an important note when looking at the results presented in this section.

Autocorrelation and periodic boundary conditions

An important note should be made on calculating the autocorrelation of a data set generated using periodic boundary conditions. The research of O’neill et al. [18] gives us some indications on the use of autocorrelation and integral timescale for a dataset based on periodic boundary conditions. Critical point in defining a reliable integral time scale is found to be in the relationship between the size of the LES-domain with its periodic boundary conditions, and the typical length scale of the clouds calculated in this research. As concluded by O’neill[18], the size of the LES domain influences the autocorrelation, and with that it influences the integral length scale. Smallest LES domain recommended to prevent this mutual influence has a length of six integral length scales.

To implement the recommendations on our own results the integral length scale is calculated by assuming that horizontal velocity is constant. The maximum integral time scale was 55 minutes. The maximum velocity in the LES model is 4.5m/s directed from south to north. In most extreme case, the integral length scale would thus have a length of $55 \times 4.5 \times 60 \approx 14.6$ km. The size of the domain is 4.5km in each direction; this means the LES-domain does not meet the recommendations of O’Neill at all. Even when using the much smaller velocity in West-East direction of 1m/s this would result in an integral

length scale of 3km.

Autocorrelation is influenced by the size of the LES domain, if the domain is not chosen big enough. Therefore, the values found in this section cannot be used to conclude anything about the time scale of the persistence.

Different points

Points A, B and C do not completely 'behave' as was expected based on their locations on the averaged time graphs. Point A was located at the highest average of liquid water path, but does not show the strongest autocorrelation if we look at variables like (virtual) potential temperature and specific total water content.

Surface plots

When looking at the integral time scale surface plots, the resemblance with the averaged plots is not convincing, though visible in the region where point B is located (South-West in the figure). Total water path and liquid water path show the strongest correlation in shape between the average figure and the integral time scale surface plot. For the vertical velocity higher integral time scales are found where the downdrafts are located. The integral timescale of the total specific water content reaches a maximum of ± 55 minutes. Vertical velocity has a very low maximum integral time scale, of 18 minutes. Other variables show maximum integral time scale varying between 38 and 48 minutes. This is slightly longer than the estimated lifetime of the shallow cumulus clouds in these data fields of 20-30 minutes.

Chapter 5

Conclusion and discussion

The main research goal of this thesis was to find persistence in a shallow cumulus cloud field. This persistence is found using time-averaging and calculating the cloud presence. One striking result from these time-averaged plots are persistent downdrafts, which are found at relatively dry locations. Next to that strong anti-correlations between q_t and (virtual) potential temperature are found. Finally, the integral time scale is calculated, resulting in a maximum integral time of 55 minutes for q_t .

Time-averaging and cloud presence

The first conclusion drawn is based on time-averaging of the different variable fields; it appeared that clouds are persistent over a significant longer time scale than their typical lifetime on this domain. Structures are persistent over the whole four hours of the LES data used, while the typical lifetime of the clouds was estimated to be 30 minutes. This persistence is clearest when looking at the total water path and the liquid water path. Virtual potential temperature, potential temperature and specific total water content show comparable results as the variables described before, but with a significant lower order compared to their original signals.

Another indication for this persistence is found in calculating the cloud presence. Cloud presence is defined as the fraction of the total time a cloud with a minimum liquid water path is present. It should be noted that this is not the consecutive time, each event a column has a liquid water path higher than the minimum, that column is 'counted' as being in-cloud. Using a minimum liquid water path of 0.1 kg.m^{-2} shows a presence of 0.27 of the total measurement time; cloud presence was more than one hour. Comparing this to the slab average cloud presence of 0.0362 gives that this is a persistent signal. If the minimum liquid water path in a cloud is 0.15 kg.m^{-2} , maximum cloud presence is 20 minutes, while the average presence of this surface was only 2 minutes. The choices of the minimum liquid water path of 0.1 respectively 0.15 kg.m^{-2} are chosen to exclude the broken stratocumulus layer also found in this domain of the ASTEX measurements from these results.

In the same scope as calculating the cloud presence, cloud fraction is defined. Using a minimum specific water content of 0.05 g.kg^{-1} cloud fraction can be calculated at each height. Therefore the eventual influence of the stratocumulus layer are excluded. A surface plot of the cloud fraction reveals us that the stratocumulus clouds do show a strong pattern also observed before in the averages.

Downdrafts

A second surprising result is found in the average over time of the vertical velocity. This average shows large persistent downdrafts of -0.2 m.s^{-1} present during 4 hours of measuring. The non averaged signal ranges between -0.5 and 0.5 m.s^{-1} . These strong downdrafts are found where liquid water path and specific total water content are low and (virtual) potential temperature is high.

Anti-correlation between q_t and θ & θ_v

In the surface plots of the time averaged figures a strong anti-correlation between specific total water content q_t and potential temperature θ is found. Since potential temperature is strongly related to virtual potential temperature θ_v , also θ_v shows a strong anticorrelation with q_t .

Autocorrelation and integral time scale

The autocorrelation of different variables ($w, \theta_v, \theta, q_t, W$ and q_r) is calculated in two ways. The first calculation is the one presented by Stull [20] and an alternative autocorrelation that uses not a varying average, but one that is the same for each time step. Both autocorrelations are calculated after detrending the variables. These two ways ([20] and the alternative one) do show comparable behaviour, although the alternative calculation results in higher values of the autocorrelation. With that, the integral time scale of this approach is maximally 30% bigger than the integral time scale calculated via Stull's approach. In order not to overestimate the integral time scale, the approach of Stull is used for further evaluation of the integral time scale.

Looking at the shape of the integral time scale surface plots at a height of 1000m, these often correlate more or less with the time-averaged figures in North-East quarter of the figures. This tells us that at least part of the previous results gives an important view on the correlation in the shallow cumulus, since stratocumulus in the ASTEX case is typically found at heights above 1200m.

Maximum calculated integral timescale varies per variable and height. Maximum overall integral timescale is 55 minutes, found for the total specific water content.

5.1 Recommendations

During this research, different things have become clear, but maybe even more questions have appeared. In this section some recommendations for further research.

- There is a strong anti correlation between the (virtual) potential temperature and total water content. However, it is not exactly clear how this anti correlation develops during the formation of a cloud, and whether these anti correlations hold both in cloud and in the environment.
- Another correlation that is interesting to look after is the one between different heights of the air. This is based on the result that the pattern as shown in the time averaged figures is reproduced when calculating the cloud fraction at the height the broken stratocumulus layer is found.
- Try to find a more continuous way to move with the mass of the air, since in these calculations not all perturbations will be excluded. This is seen in the visual inspection of the cloud fields.
- Calculate these autocorrelation in a larger domain to be sure to exclude the influence of the periodic boundary conditions. The exact size of the domain is difficult to guess. Following the research of O'Neill, the domain should have a range of 8 times the integral length scale. In our case this means that the domain should

be about 100km in each horizontal direction to gain reliable results on the autocorrelation and integral time scale. This domain range estimation is based on the integral time scale found in this research. In this way influence of the periodic boundary conditions on the autocorrelation will be minimized.

Abbreviations

list of used abbreviations:

ASTEX	Atlantic Stratocumulus Transition Experiment
CIN	Convective Inhibition
DALES	Dutch Atmospheric Large Eddy Simulation
LFC	Level of Free Convection
LNB	Level of Neutral Buoyancy
RH	Relative Humidity
LCL	Lifting Condensation Level

Symbols

List of used symbols:

symbol	unit	variable
α	m^3kg^{-1}	specific volume
c_p	$\text{Jkg}^{-1}\text{K}^{-1}$	specific heat of air at constant pressure
$c_t(x, y)$	-	cloud cover at point (x, y)
e	Pa	partial vapor pressure
e_s	Pa	saturation water vapor pressure
ϵ	-	R_d/R_v
Δt	s	variable time step relating τ with n_τ
F_B	N	buoyant force
g	ms^{-2}	gravitational acceleration
Γ_d	Km^{-1}	dry adiabatic lapse rate
Γ_m	Km^{-1}	wet adiabatic lapse rate
H	m	height of a cloud
$I(x, y)$	-	binar representation of the point (x, y) , at each point $I=1$
$I_c(x, y)$	-	binar representation; $I_c = 1$ if (x, y) is in cloud
K	$\text{m}^2.\text{s}^{-1}$	eddy diffusivity constant
L_v	kJkg^{-1}	latent heat release of vaporization, in this project of water
p	Pa	pressure
p_d	Pa	pressure of dry air
q_i	kg.kg^{-1}	specific ice content
q_l	kg.kg^{-1}	specific liquid water content
q_s	kg.kg^{-1}	saturated liquid water content
q_t	kg.kg^{-1}	specific total water content
q_v	kg.kg^{-1}	specific vapor content
R^*	$\text{J.K}^{-1}.\text{mol}^{-1}$	universal gas constant
R_d	$\text{J.K}^{-1}.\text{kg}^{-1}$	gas constant for dry air

symbol	unit	variable
r_{sat}	-	mixing ratio of water vapor with air at saturation vapor pressure
R_m	$J.K^{-1}.kg^{-1}$	gas constant for moist air
R_v	$J.K^{-1}.kg^{-1}$	gas constant for vapor
ρ	$kg.m^{-3}$	density
ρ_{air}	$kg.m^{-3}$	density of air
$\rho(\tau)$	-	autocorrelation at time lapse τ
S_ψ	-	factor containing all important processes influencing ψ
T	K	temperature
T	s	typical lifetime of the cumulus clouds
T_v	K	virtual temperature
TW	$kg.m^{-2}$	total water path
θ	K	potential temperature
θ_e	K	equivalent potential temperature
θ_l	K	liquid water potential temperature
θ_v	K	virtual potential temperature
τ	s	time step between two compared moments
τ_{int}	s	integral timescale
m	m	mass
n	mol	number of moles
n_τ	-	number of timesteps used for the autocorrelation
$n_{\tau_{max}}$	-	total number of timesteps used for the autocorrelation
Φ	$J.kg^{-1}$	gravitational potential energy per unit mass
u	$m.s^{-1}$	velocity in x (East-West) direction
v	$m.s^{-1}$	velocity in y (South-North) direction
V	m^3	volume
ψ	-	function of θ_l and q_t used in LES modeling
W	$kg.m^{-2}$	liquid water path
w	$m.s^{-1}$	vertical velocity
w_*	$m.s^{-1}$	convective velocity scale
x_n	m	location of point n before lagrangian correction of the 3D fields
x'_n	m	location of point n after lagrangian correction of the 3D fields

Bibliography

- [1] B. Albrecht et al., C. Bretherton, D. Johnson, W. Scubert, and A. Shelby Frish, “The atlantic stratocumulus transition experiment – astex,” *Bulletin oof the American Meteorological Society*, vol. 76, pp. 889–904, June 1995.
- [2] S. de Roode and P. Duynkerke, “Dynamics of cumulus rising into stratocumulus as observed during the first ‘lagrangian’ experiment of astex,” *Quarterly Journal of the Royal Meteorological Society*, no. 122, pp. 1597–1623, 1996.
- [3] J. van der Dussen and S. de Roode, “Persistent turbulence structures and their relation to cumulus cloud formation.” project description at TUD website, -.
- [4] J. van der Dussen, “Large eddy and mixed-layer model simulations of the stratocumulus to cumulus transition as observed during astex,” Master’s thesis, Delft University of Technology, September 2009.
- [5] J. Dawe and P. Austin, “Statistical analysis of an les shallow cumulus cloud ensemble using a cloud tracking algorithm,” *Atmospheric Chemistry and Physics*, no. 12, pp. 1101–1119, 2012.
- [6] J. Wallace and P. Hobbs, *Atmospheric Science*, ch. Atmospheric Thermodynamics, pp. 63–102. Academic Press, second ed., 2006.
- [7] S. de Roode, “Clouds,” (http://www.srderoode.nl/index.php?option=com_content&view=article&id=68&Itemid=79), September 2004.
- [8] S. Looijen Axelsen, “The role of relative humidity on shallow cumulus dynamics; results from a large eddy simulation model,” Master’s thesis, Delft University of Technology, April 2005.
- [9] J. Wallace and P. Hobbs, *Atmospheric Science*, ch. Introduction and Overview, p. 8. Academic Press, second ed., 2006.
- [10] J. Wallace and P. Hobbs, *Atmospheric Science*, ch. Introduction and Overview, pp. 97–98. Academic Press, second ed., 2006.
- [11] S. de Roode, “The effect of temperature and humidity fluctuations on the liquid water path of non-precipitating closed-cell stratocumulus clouds,” *Quarterly Journal of the Royal Meteorological Society*, no. 134, pp. 403–416, 2008.
- [12] JK, “Clouds, clouds and music.” personal blog, <http://barbados2010-actos.blogspot.com/2010/11/clouds-clouds-and-music.html>, november 2010.
- [13] R. Rogers and M. Yau, *A short course in cloud physics*. Butterworth-Heinemann, third ed., 1989.
- [14] J. Cuijpers and P. Duynkerke, “Large eddy simulation of trade wind cumulus,” *Journal of the Atmospheric Sciences*, vol. 50, no. 23, pp. 3894–3908, 1993.
- [15] S. de Roode and J. van der Dussen, “Large-eddy simulation of a stratocumulus to cumulus cloud transition as observed during astex,” MSP, Delft University of Technology.

- [16] T. Heus, C. Van Heerwaarden, H. Jonker, A. Siebesma, S. Axelsen, K. van den Dries, O. Geoffroy, A. Moene, D. Pino, S. de Roode, *et al.*, “Formulation of the dutch atmospheric large-eddy simulation and overview of its applications,” *Geoscientific Model Development*, vol. 3, pp. 415–444, 2010.
- [17] R. Stull, *An Introduction to Boundary Layer Meteorology*, ch. Some Mathematical and Conceptual Tools: Part 2 Time series, pp. 296–299. Kluwer Academic Publishers, 1988.
- [18] P. O’Neill, D. Nicolaides, D. Honnery, and J. Soria, “Autocorrelation functions and the determination of integral length with reference to experimental and numerical data.” 15th Australasian Fluid Mechanics Conference, December 2004.
- [19] Euclipse, “Set up of the astex large-eddy simulation.” internet, http://www.euclipse.nl/wp3/ASTEX_Lagrangian/LES_astex_setup.shtml, -. European Unuin Cloud Intercomparison, Process Study and Evaluation Project.
- [20] R. Stull, *An Introduction to Boundary Layer Meteorology*, pp. 118,355. Kluwer Academic Publishers, 1988.
- [21] K. Trenberth, “Some effects of finite sample size and persistence on meteorological statistics. part i: Autocorrelations,” *Monthly weather review*, no. 112, pp. 2359–2368, 1984.

Appendix A

Time-averaged profiles

In this appendix, the extensive results of section 3.4 are provided. The following figures all represent one variable at a height of 600m, averaged over one hour of the total four hours the 3D data fields cover in this project.

A.1 Specific total water content

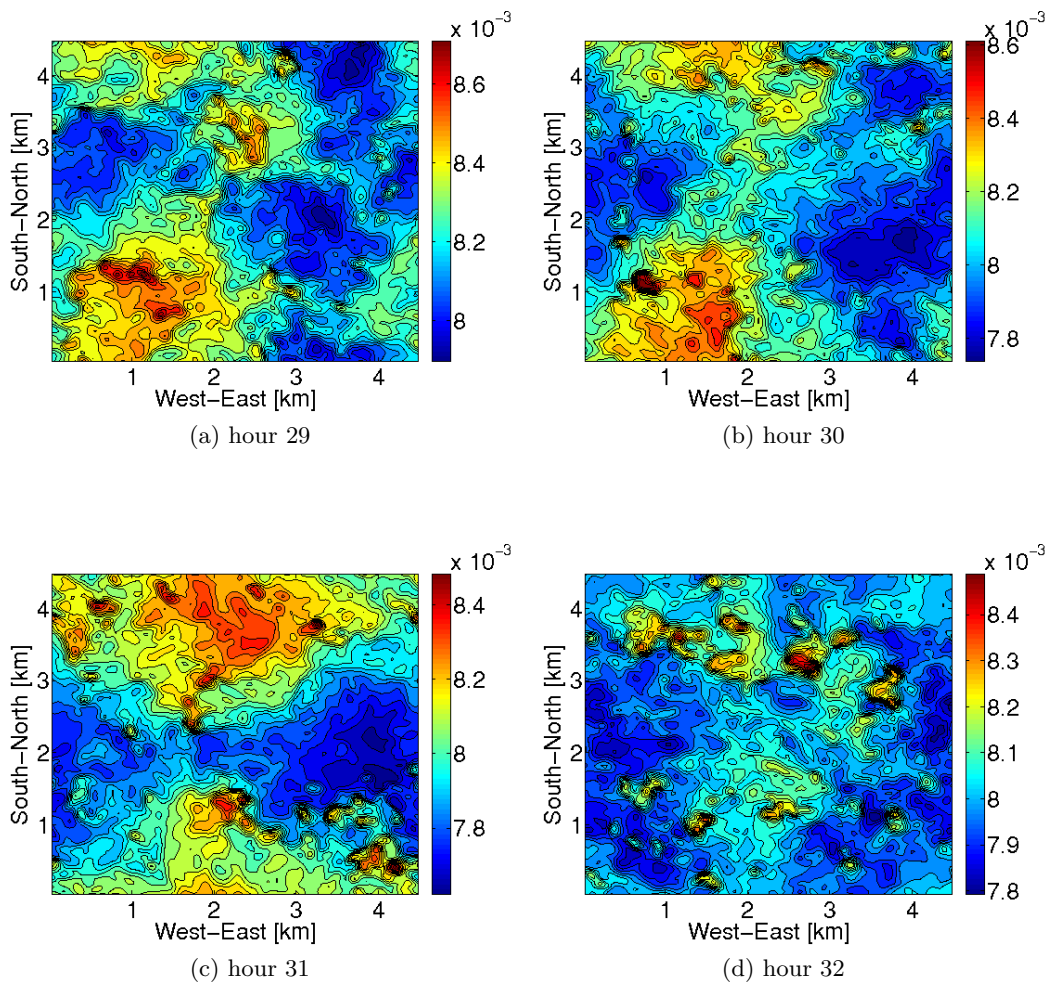


Figure A.1.1: q_t averaged in time for four different timesteps at a height of 1km.

A.2 Specific rain content

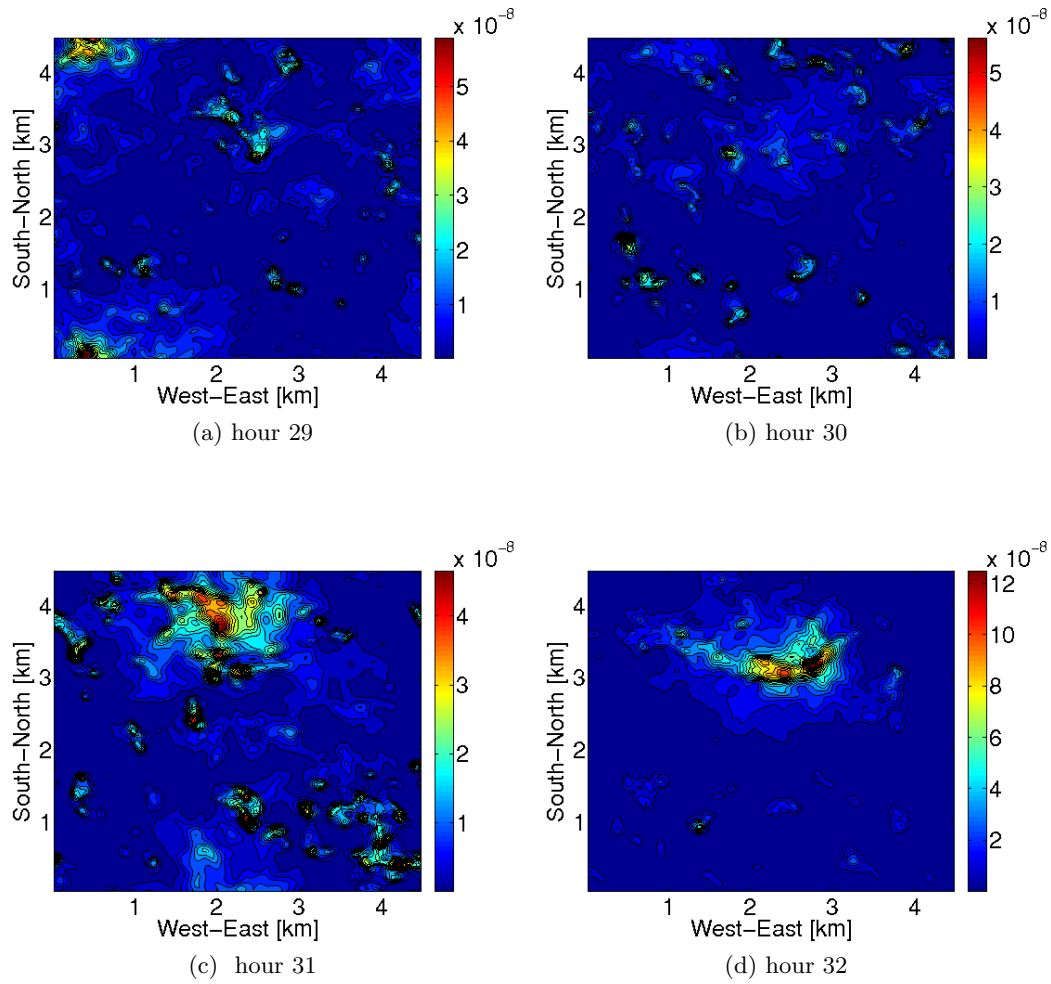


Figure A.2.1: q_r averaged in time for four different timesteps at a height of 1km.

A.3 Potential temperature

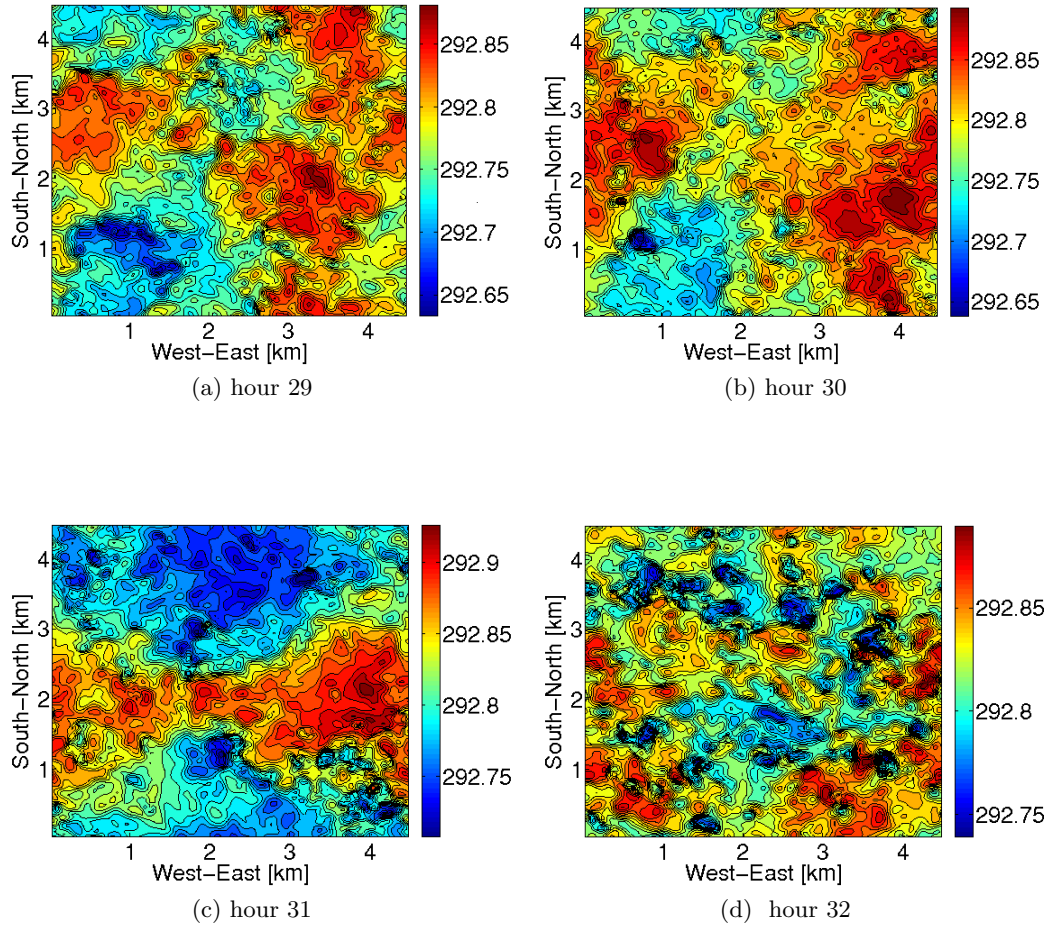


Figure A.3.1: θ averaged in time for four different timesteps at a height of 1km.

A.4 Virtual potential temperature

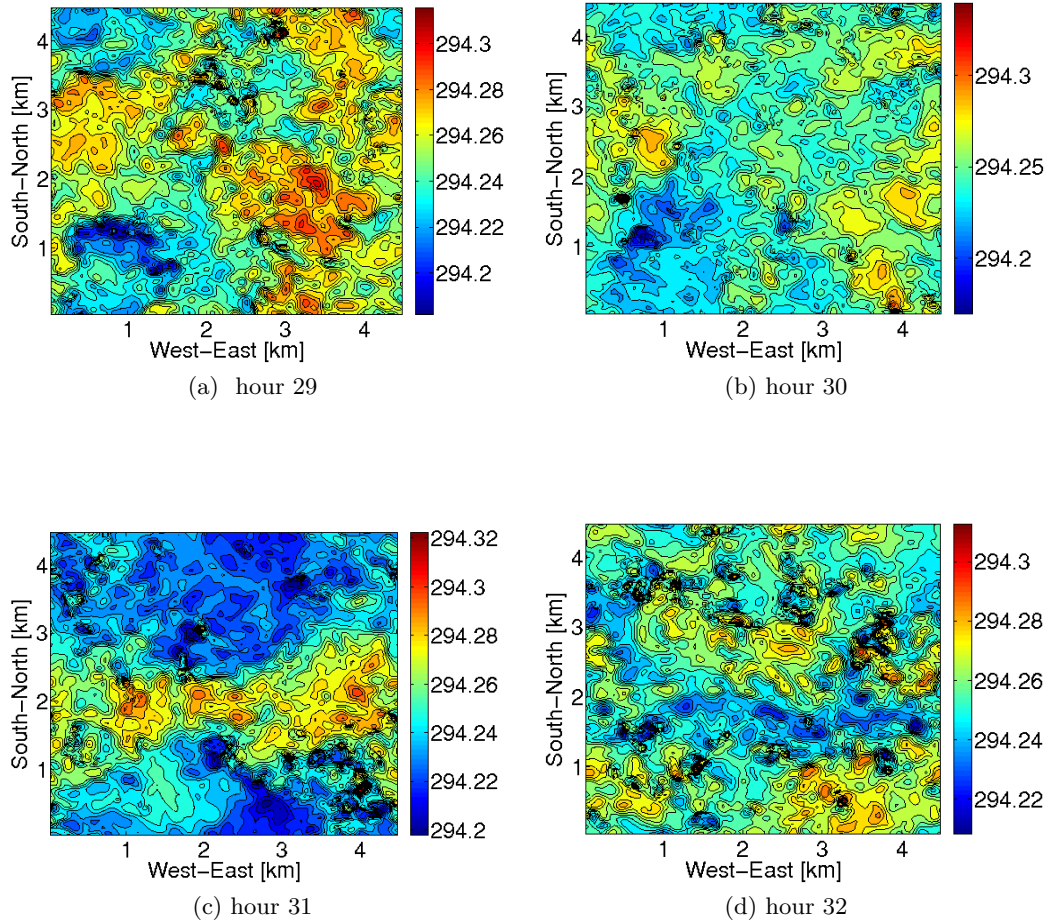


Figure A.4.1: θ averaged in time for four different timesteps at a height of 1km.

A.5 Vertical velocity

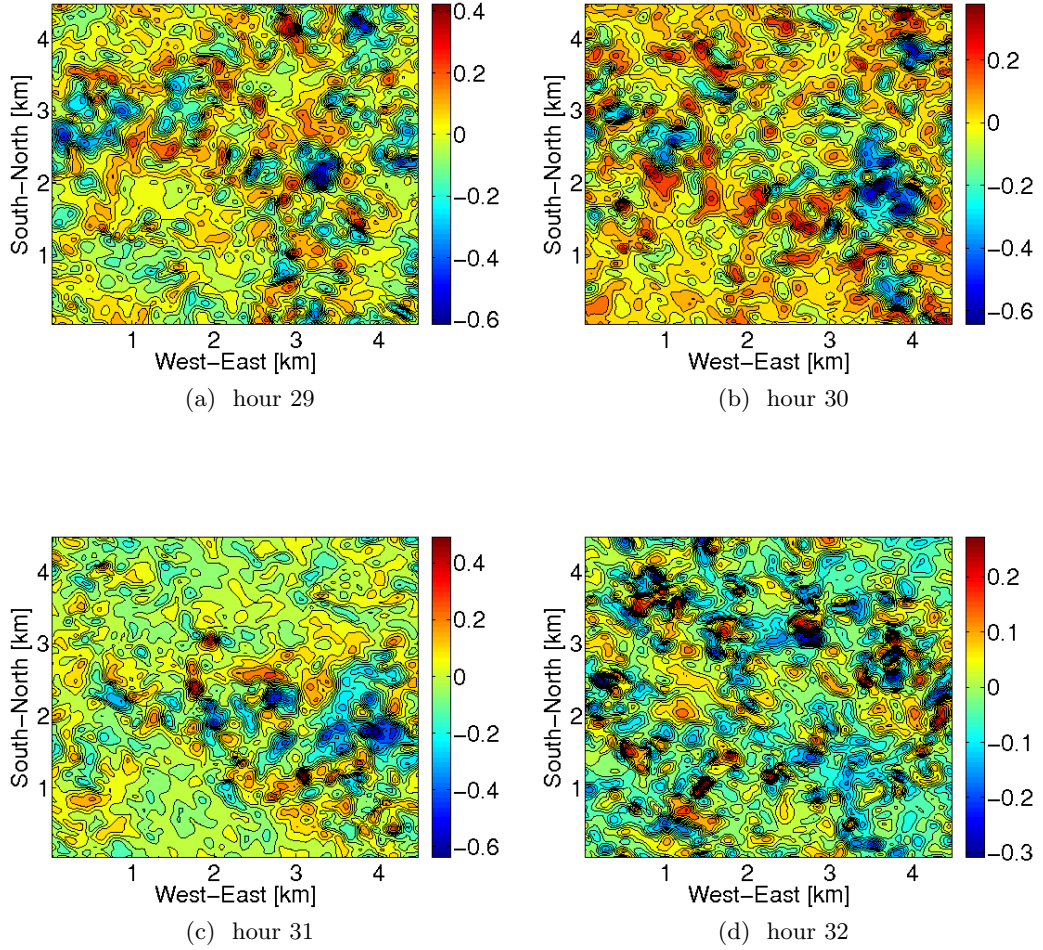


Figure A.5.1: Vertical velocity w averaged in time for four different timesteps at a height of 1km.

A.6 Total water path

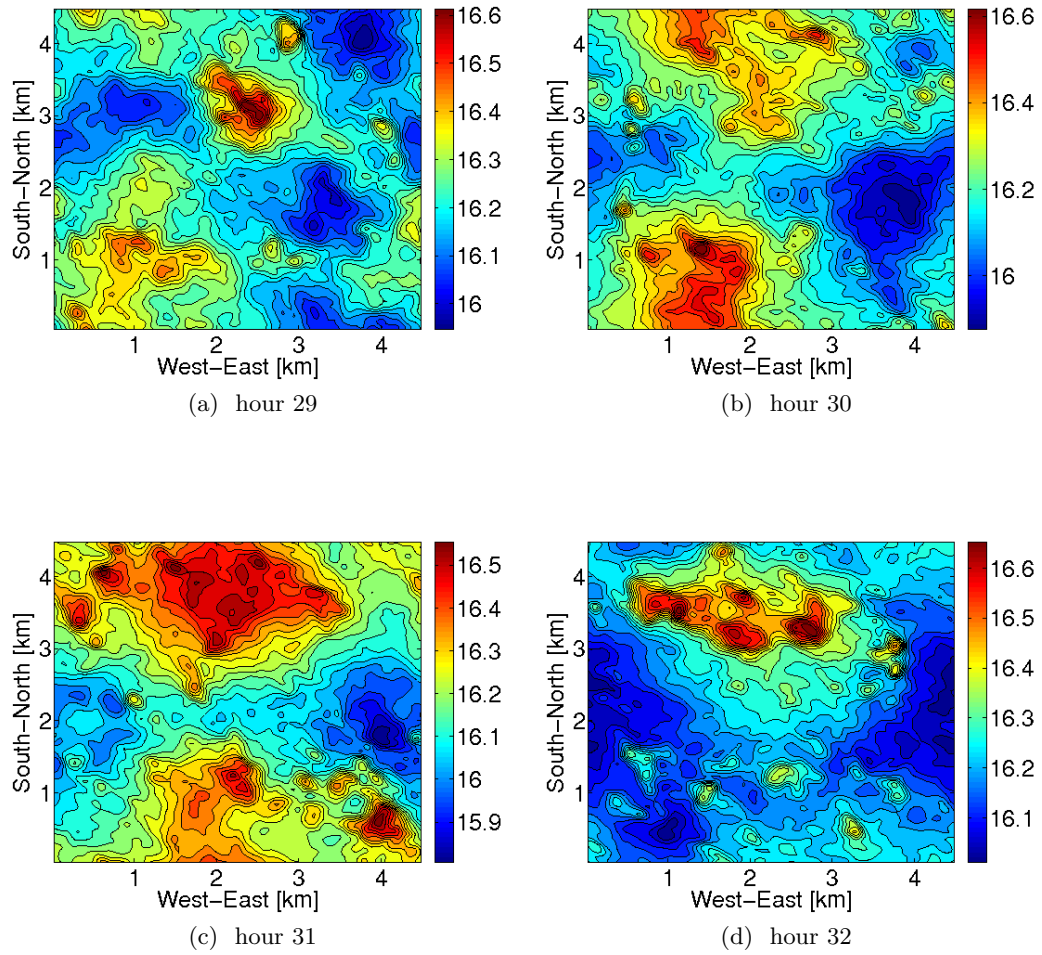


Figure A.6.1: Total liquid water path TW averaged in time for four different timesteps.